

Review

# Advanced Nickel-Based Catalysts for Urea Oxidation Reaction: Challenges and Developments

Yaming Ma <sup>1</sup>, Chenxiang Ma <sup>1</sup>, Yingche Wang <sup>1</sup> and Ke Wang <sup>2,\*</sup>

<sup>1</sup> Xi'an Institute of Electromechanical Information Technology, Xi'an 710075, China; mayamingxjtu@hotmail.com (Y.M.); chenxiangma@tju.edu.cn (C.M.); yingchewang212@hotmail.com (Y.W.)

<sup>2</sup> Xi'an Key Laboratory of Sustainable Energy Materials Chemistry, School of Chemistry, Xi'an Jiaotong University, Xi'an 710049, China

\* Correspondence: mxbk19950604@stu.xjtu.edu.cn

**Abstract:** The electrochemical urea oxidation reaction (UOR) is crucial for determining industrial and commercial applications of urea-based energy conversion devices. However, the performance of UOR is limited by the dynamic complex of the six-electron transfer process. To this end, it is essential to develop efficient UOR catalysts. Nickel-based materials have been extensively investigated owing to their high activity, easy modification, stable properties, and cheap and abundant reserves. Various material designs and strategies have been investigated in producing highly efficient UOR catalysts including alloying, doping, heterostructure construction, defect engineering, micro functionalization, conductivity modulation, etc. It is essential to promptly review the progress in this field to significantly inspire subsequent studies. In this review, we summarized a comprehensive investigation of the mechanisms of oxidation or poisoning and UOR processes on nickel-based catalysts as well as different approaches to prepare highly active catalysts. Moreover, challenges and prospects for future developments associated with issues of UOR in urea-based energy conversion applications were also discussed.



**Citation:** Ma, Y.; Ma, C.; Wang, Y.; Wang, K. Advanced Nickel-Based Catalysts for Urea Oxidation Reaction: Challenges and Developments. *Catalysts* **2022**, *12*, 337. <https://doi.org/10.3390/catal12030337>

Academic Editor: Nicolas Alonso-Vante

Received: 11 January 2022

Accepted: 4 March 2022

Published: 16 March 2022

**Publisher's Note:** MDPI stays neutral with regard to jurisdictional claims in published maps and institutional affiliations.



**Copyright:** © 2022 by the authors. Licensee MDPI, Basel, Switzerland. This article is an open access article distributed under the terms and conditions of the Creative Commons Attribution (CC BY) license (<https://creativecommons.org/licenses/by/4.0/>).

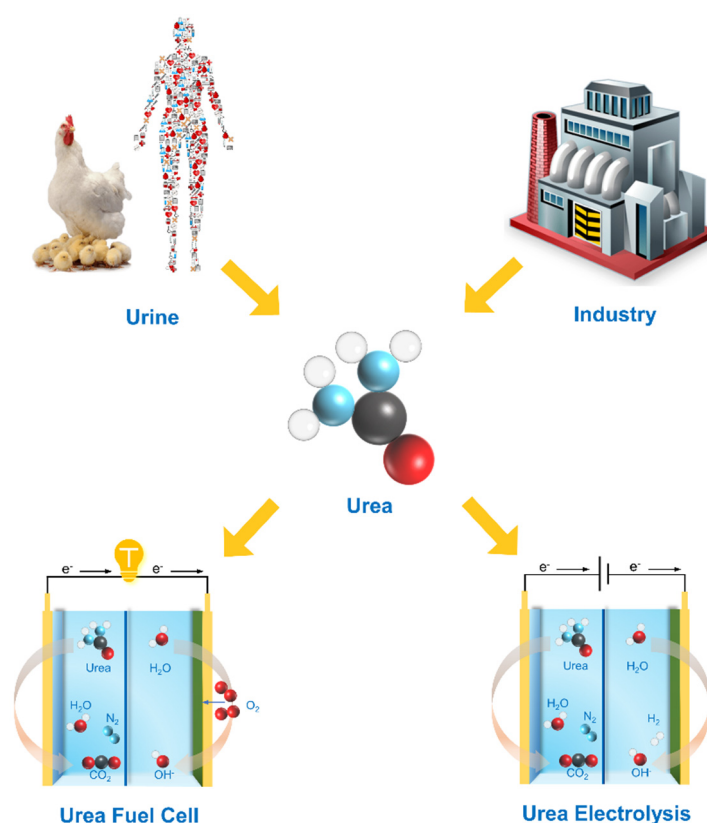
**Keywords:** nickel-based catalysts; urea oxidation reaction; direct urea fuel cells; energy conversion; nanocomposites

## 1. Introduction

Urea, a type of nontoxic organic compound that contains carbon, nitrogen, oxygen, and hydrogen elements, is used as an extremely important nitrogenous fertilizer in agricultural production [1,2]. From a biomedical view, it is an important component in urine; as a metabolite of the human body, it is an important metabolic substance [3]. The amount of urea is closely associated with the health of individuals [4]. Precise early-stage detection of urea in urine plays a significant role in medical diagnosis as it can effectively indicate the status of the human body [5,6]. In terms of environmental pollution, large quantities of untreated wastewater contaminated with urea, including industry production and human as well as animal urine, can cause serious environmental problems as it decomposes into ammonia with nitrogen-based pollutants (e.g., NO, NO<sub>2</sub>) [7–9]. Urea as an energy carrier is non-flammable, easily stored and transported, and has an energy density of 16.9 MJ L<sup>-1</sup> which is 10 times than that of hydrogen. From an energy utilization perspective, it can release huge amounts of energy when used for fuel combustion [10,11]. Therefore, effective detection, treatment, and consumption of urea is of great significance to industrial production, environmental treatment of urea-rich wastewater, and even healthcare [12,13].

Traditional urea treatments including adsorption [14–17], hydrolysis [18,19], biodegradation [20,21], and chemical oxidation [22–24] require excessive energy consumption and high-cost equipment-dependent processing, which greatly inhibit broader applications of these methods. These methods are not cost effective or sustainable for the development of green economies [25–27]. With the development of advanced technology and research,

electrolysis of urea has become a powerful method that takes advantages of the facile working, huge processing capacity, and non-toxic production of  $\text{CO}_2$ ,  $\text{N}_2$ , and  $\text{H}_2\text{O}$  [28,29]. More than that, the electrocatalysts in UOR processing can easily be realized without the utilization of noble metals under alkaline solution, which immensely reduces the cost and increases the possibility of catalyst application. On the other hand, UOR can be performed for direct urea fuel cell (DUFC) using an anodic reaction, which converts the chemical energy of urea directly into electricity [30–32]. During the above procedure, the urea-rich industrial wastewater or even human or animal urine can be added as electrolytes to achieve simultaneous wastewater treatment and electricity generation (Scheme 1) [33–36]. Brief and basic chemical reactions in DUFC can be classified by the following equations:



**Scheme 1.** An illustration of urea-based energy conversion systems, including urea electrolysis and urea fuel cell.

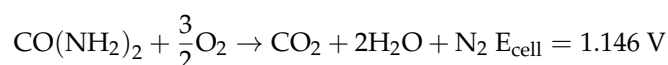
Cathodic reaction:



Anodic reaction:



Overall reaction:



From the above equations, the DUFC has high open-circuit voltage (OCV) with 1.146 V and a high theoretical efficiency of 102.9% because of other factors such as absorption heat from surrounding environments [37–39].

For electrocatalysts, nickel-based materials are considered the best non-noble catalysts, with promising applications for UORs in alkaline electrolytes [9,40–42]. Owing to the activity and durability of nickel-based materials, they are far from wide commercialization [43–46]. The basic principles and rules that are commonly used in designing nickel-based materials to improve electrocatalysis performance are as follows: (i) increasing activity by alloying with other metals; (ii) increasing intrinsic catalytic activity and sites by complexing with other inorganic elements and microstructure designs; and (iii) increasing the surface area to improve activity and stability by complexing with carbon composites.

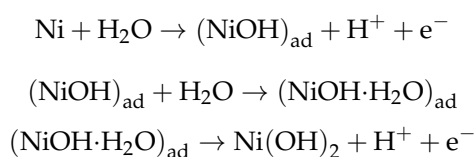
Based on literature sample survey data, the research field still lacks a comprehensive and in-depth summary of state-of-the-art design and synthesis strategies of nickel-based catalysts for UOR. Therefore, this review starts with the electrochemical characteristics of nickel in alkaline media and summarizes the recent progress in designing concepts and basic principles of nickel-based materials from elaborately selected examples with detailed discussions in the following sections. This review emphasizes the catalytic mechanism as not just an intuitive statistic result of UOR performance. Challenges and development are presented for research avenues to use advanced UOR catalysts.

## 2. Mechanism of UOR in Alkaline Media on Ni-Based Catalysts

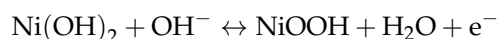
Nickel-based catalysts have been widely applied in electro-oxidation of urea as alternatives to precious metals. Therefore, understanding the mechanism processing of UOR in alkaline media is key for preparing highly active catalysts.

### 2.1. The Oxidation and Electrochemical Oxidation of Metallic Nickel

As a more active element than copper, Ni corrodes spontaneously into thin-layer structures of NiO/Ni(OH)<sub>2</sub> in humid air following the below equations:



During cyclic voltammetry of metallic Ni electrodes in alkaline solution (typical KOH), the NiO/Ni(OH)<sub>2</sub> layers expand with OH<sup>−</sup> adsorbed on the surface of intrinsic thin layers under positive scan at a high voltage. The NiOOH layer eventually forms as a result of penetration of OH<sup>−</sup> into NiO/Ni(OH)<sub>2</sub> layers at a higher voltage. A typical oxidic peak occurs around 1.45 V vs. RHE along with the maximum current achieved in the reversible Ni<sup>2+</sup>/(Ni(OH)<sub>2</sub>)/Ni<sup>3+</sup>/(NiOOH) transformation following the below equation:



The metastable hydrous α-Ni(OH)<sub>2</sub> slowly converts into stable anhydrous β-Ni(OH)<sub>2</sub> with forward scan at a high voltage. The latter is partially oxidized to form γ-NiOOH around 380 mV vs. Hg/HgO and accumulated on the surface of Ni electrodes. Accordingly, γ-NiOOH is reduced to corresponding β-Ni(OH)<sub>2</sub> under backward scan. A significant current increase occurs at voltages higher than 380 mV vs. Hg/HgO in alkaline urea solutions, indicating that γ-NiOOH can be an active substance. Hence, higher anodic peak voltage with positive scan indicates lower activity against poisoning, but lower anodic peak voltage indicates higher catalytic activity. Meanwhile, KOH was found to be the better electrolyte for UOR compared to LiOH or NaOH, since K<sup>+</sup> ions promote performance of UOR by releasing C–O bonds and facilitating the detachment of CO<sub>2</sub> which is a rate-determining step in UOR. UOR over Ni catalysts in alkaline solutions occurs through two pathways, direct or indirect, as follows:

1. The direct mechanism was proposed by Vedharathinam et al. using potential-dependent in situ surface-enhanced Raman spectroscopy technology. As shown in Figure 1A, two distinct peaks of Ni<sup>−</sup>–O bending and stretching appeared on 479 and 559 cm<sup>−1</sup> at 300 mV vs. Hg/HgO

in urea-free KOH electrolytes indicating NiOOH formation. Meanwhile, the two peaks lost intensity if voltage peaked above 520 mV vs. Hg/HgO, suggesting an OER instead of an oxidation reaction. The original peaks shifted to 476 and 558  $\text{cm}^{-1}$  and new peaks of symmetric urea C–N stretch arose at 1003  $\text{cm}^{-1}$  that decreased in intensity with increasing voltage, indicating UOR on NiOOH. The  $\text{CO}_2$  produced by UOR and dissolved in solution was confirmed by detection  $\text{CO}_3^{2-}$  at 1062  $\text{cm}^{-1}$  at 500 mV vs. Hg/HgO. The postulated reaction processes are shown in the following equations:

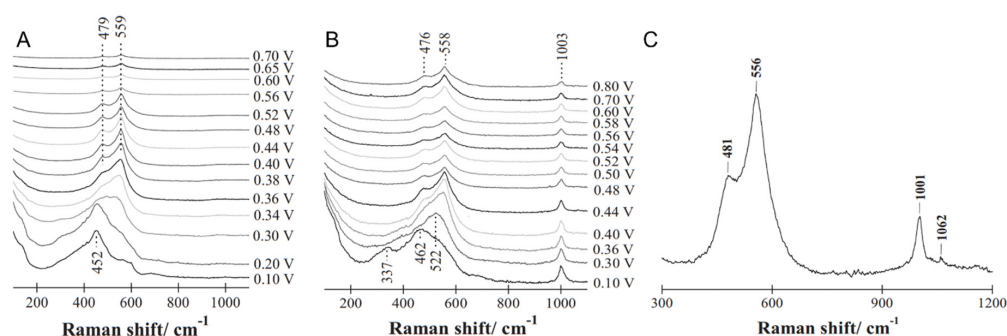
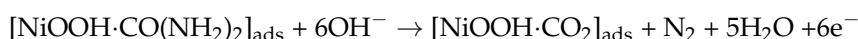
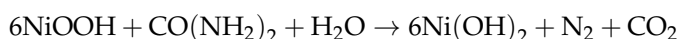
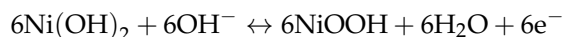


**Figure 1.** In situ surface-enhanced Raman spectra of  $\text{Ni}(\text{OH})_2$  with different potentials and solutions: (A) urea-free 5 mol  $\text{L}^{-1}$  KOH, (B) 5 mol  $\text{L}^{-1}$  KOH with urea, and (C) 5 mol  $\text{L}^{-1}$  KOH with urea [47]. Reproduced with permission [47]. Copyright 2013, Elsevier Ltd.



2. The indirect mechanism via catalyst regeneration assumes that active sites of NiOOH oxide to form  $\text{Ni}(\text{OH})_2$  in reaction with urea, which results in loss of the active sites. The postulated processes are shown in the following equations:



## 2.2. Inactivation or Poisoning of Nickel-Based Catalysts

The intermediate of CO or  $\text{CO}^*$  produced in UOR processing can be easily and strongly absorbed by nickel-based catalysts and block active sites, from which inactivation or poisoning occurs [36]. Common methods such as cyclic voltammetry and polarity switching have been used to recover active sites. Vase et al. discovered that Ni could be activated by polarity switching at 1 min intervals 4 times with two cycles of 2 min intervals and maintaining catalysts when worked as anode for 1 h. In addition, the activity and stability of Ni-based catalysts could be significantly improved by increasing the temperature during the aforementioned activation process from 33 to 66  $^\circ\text{C}$  or adding LiOH into electrolytes. Other methods such as cyclic voltammetry also regenerate activity through desorption of the surface species for intermediates of CO or  $\text{CO}^*$  in reverse scan.

In the following section, we introduce various methods to enhance the activity of Ni-based catalysts through alloying, oxidation, or composite to achieve the current density, decrease onset potential or anodic peak potential, etc.

### 3. Tailoring Ni-Based Catalysts for UOR

Alloying different metals such as hybrids with non-metal elements or composites with other metallic oxides is a common strategy to enhance catalytic activity of Ni-based catalysts [30–48]. A few studies have investigated non-Ni-based catalysts. The typical three electrode system is used to evaluate the activity of UOR and which catalyst directly or indirectly supports highly conductive substrates such as glass carbon, nickel foam, and carbon cloth as work electrode, reference electrode (Ag/AgCl, Hg/HgO, or Hg/HgSO<sub>4</sub>), and counter electrode (Pt plat, mesh, wire or carbon rod) [12].

#### 3.1. Other Metals Compounded with Nickel Hydroxides

There have been many endeavors to design hierarchical layered double hydroxides (LDHs), especially Ni(OH)<sub>2</sub> including  $\alpha$  or  $\beta$  types which are nanostructures that have been widely used in UOR with abundant edge sites. However, the low electronic conductivity and relatively sparse catalytic edge sites of Ni(OH)<sub>2</sub> limits its catalytic activity. Physicochemical structural modification has been used to improve its conductivity and catalytic activity, such as interlayer charge compensating with different inorganic or organic anions (NO<sub>3</sub><sup>−</sup>, CO<sub>3</sub><sup>2−</sup>, Cl<sup>−</sup>, SO<sub>4</sub><sup>2−</sup>, etc.), embedding various valence transition metal-based ions into layered structures and thus changing the molar ratio of M<sup>2+</sup>/M<sup>3+</sup>. Wang et al. fabricated a novel hybrid 3D hierarchical architecture on porous NF, a fullerene quantum dot-decorated CoNi-LDH nanosheet (noted FQD/CoNi-LDH/NF), by a one-step self-assembly process for both water splitting and UOR. Benefitting from the advantage of synergistic effects between FQD and CoNi-LDH and the inherent activity of CoNi-LDH, the as-obtained exhibited impressive activity for overall urea electrolysis (Figure 2A). The catalyst required only 1.59 and 1.45 V to achieve 10 mA cm<sup>−2</sup> for water or urea electrolysis as both anode and cathode [49]. Xie et al. designed hierarchical wire-on sheet Ni(OH)<sub>2</sub> nanoarrays with optimal cerium (Ce) doping and tailoring phase regulation (Ce: $\alpha$ -Ni(OH)<sub>2</sub>) via the hydrothermal method in Ni/Ce salts with urea in presence on NF, which showed high performance for UOR (Figure 2B). Detailed characterization indicated that  $\alpha$ -Ni(OH)<sub>2</sub> with local Ni<sup>3+</sup> species provides higher inherent UOR activity than  $\beta$ -phase and further promoted via Ce-doping [50]. Kim et al. demonstrated amorphous and porous 2D NiFeCo-LDH directly grown on NF by the electrodeposition method for efficient electrolysis of both UOR and water splitting (Figure 2C). Porous confinement in 2D orientation and amorphous and synergistic effects resulted in the excellent performance, where current density of 10 mA cm<sup>−2</sup> for overall water splitting required 1.57 V in 1 M KOH and 0.280 V (vs. SCE) to drive 10 mA cm<sup>−2</sup> for UOR [51]. Cao et al. proposed a hierarchical triple-layered heterostructure with NF as the bottom layer, Ni(OH)<sub>2</sub> as the top layer, and MnCo<sub>2</sub>O<sub>5</sub> nanosheet in the middle via direct hydrothermal, calcination, and hydrothermal processes (noted as MnCo<sub>2</sub>O<sub>5</sub>@Ni(OH)<sub>2</sub>/NF) (Figure 2D). The unique interlayer structure and synergistic effects between the three parts facilitated the transfer of ions and molecules and the rapid release of gas; the catalyst presented superior performance for UOR, achieving 650 mA cm<sup>−2</sup> and a small onset potential of 0.19 V (vs. Ag/AgCl) in 5 M KOH and 0.33 M urea electrolyte [52]. Wang et al. reported that Ni(OH)<sub>2</sub> or nanosheets and nanowire directly grew on NF (noted as Ni(OH)<sub>2</sub> NS@NW/Ni foam) via a surface engineering strategy using 3D anodic electrodes for superior urea electrolysis (Figure 2E). The integrated electrode afforded a current density of 10 mA cm<sup>−2</sup> on a potential of 0.34 V (vs. SCE) in alkaline electrolytes with urea, surpassing most reported UOR catalysts [53]. Yang et al. systematically synthesized NiCo layered double hydroxide (NiCo-LDH) with different intercalant such as NO<sub>3</sub><sup>−</sup>, CO<sub>3</sub><sup>2−</sup>, and Br<sup>−</sup> (Figure 2F). Electrocatalytic results for NiCo-LDH with NO<sub>3</sub><sup>−</sup> intercalant showed the best electrocatalytic performance and selectivity along with low onset potential and high faradaic efficiency and durability for UOR. The characterization of structure revealed that larger spacings play a pivotal role in high activity and selectivity for UOR [54]. Zhang et al. proposed a novel material of MoP@NiCo-LDH/NF on NF for a bifunctional electrocatalyst that is synthesized via phosphorylation after NF hydrothermal reaction with ammonium molybdate followed

by electrodeposition with solutions containing Ni and Co ions. Electrochemical results indicated that MoP@NiCo-LDH/NF-20 had better performance than others for water splitting and UOR, which only needs 1.405 V to achieve  $100 \text{ mA cm}^{-2}$  [55]. Dau et al. explored the structural effect of Mn in NiMn nanostructures containing different Mn ion decompositions on carbon fiber paper (CFP) via the ultrasonic radiation method following treatment by electrochemical deposition of the Ni-oxyhydroxide layer (for Ni) (Figure 2G). The strong intimate contact between CFP and the catalyst led to highly efficient charge and mass transfer, which was an advantage for urea electrocatalysis. The study provided a mechanistic avenue for designing and fabricating Ni-based catalysts with high activity [56]. Gu et al. designed ultrafine-grained NiCo-LDH nanosheets with partial exfoliation via structural engineering involving transforming unstable EDTA-intercalated NiCo-LDH into stable  $\text{NiCo-CO}_3^{2-}$ -LDH in 1 M KOH as electrocatalysts for UOR. The incorporation of Co content effectively improved conductivity, exposed numerous accessible crystal edge sites on the basal plane, and promoted the  $\text{Ni}^{3+}/\text{Ni}^{2+}$  redox reaction. In addition, the catalyst delivered a current density of  $10 \text{ mA cm}^{-2}$  only at the potential of 0.341 V vs. Hg/HgO [57]. Zhang et al. designed Co element-doped  $\text{Ni}(\text{OH})_2$  hybrid films (noted as  $\text{Co}_x\text{-Ni}(\text{OH})_2$  NPs/CF) that assembled 3D networks on Cu foam with ultrafine nanoparticles efficiently for both urea-assisted overall water splitting. The systematic investigation found that the content of Co-doped films not only influenced the morphological structure with abundant activity sites but also modified the electronic structure of host films, providing lower onset potential for UOR [58]. Wu et al. fabricated hierarchical, porous, and ultrathin  $\text{Ni}(\text{OH})_2$  nanostructures that are grown in situ on NF as high-performance and stability electrocatalysts for UOR ( $\text{Ni}(\text{OH})_2\text{/NF}$ ). Consequently, the electrode provided a current density of  $10 \text{ mA cm}^{-2}$  at 1.35 V vs. RHE [59]. Tang et al. designed hierarchical Cu-incorporated  $\alpha\text{-Ni}(\text{OH})_2$  nanoarrays as high performance electrocatalysts for both water splitting and UOR. Benefitting from the unique 1D-2D-3D structure, the catalyst provided abundant activity sites, fast charge and mass transporting, and pre-oxidation processes of  $\text{Ni}^{3+}$  to  $\text{Ni}^{2+}$  [60].

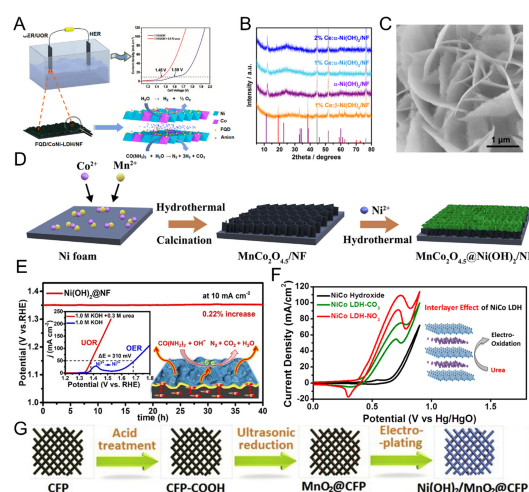


**Figure 2.** (A) FQD/CoNi-LDH/NF catalysts for efficient water and urea splitting [49]. Reproduced with permission [49]. Copyright 2020, Elsevier B.V. (B,C) XRD patterns and SEM images of the sample [50]. Reproduced with permission [50]. Copyright 2019, American Chemical Society. (D) Illustration of triple-layered  $\text{MnCo}_2\text{O}_{4.5}\text{/Ni}(\text{OH})_2\text{/NF}$  nanosheet arrays [52]. Reproduced with permission [52]. Copyright 2020, Elsevier B.V. (E) TOC of ultrathin  $\text{Ni}(\text{OH})_2$  nanostructures on nickel foam [53]. Reproduced with permission [53]. Copyright 2018, Elsevier Ltd. (F) TOC of NiCo layered double hydroxide for promoted UOR [54]. Reproduced with permission [54]. Copyright 2019, American Chemical Society. (G) Schematic illustration of the synthesizing procedures for the CFP- $\text{Ni}(\text{OH})_2\text{/MnO}_2$  film [56]. Reproduced with permission [56]. Copyright 2019, Elsevier Ltd.

### 3.2. Alloying Nickel-Based Catalysts

The activity of nickel-based catalysts for UOR are dramatically improved by alloy and structure modification with other metals such as noble metals Pt [61], Ru, Ag, Pd, Au, Ir, and Rh [62], and non-noble metals such as nickel-based NiCo [63–67], NiMn [68–70], NiZn [71,72], NiWC [73,74], NiFe [75,76], NiCd [77], and NiCr [78,79]. The alloyed nickel-based catalysts significantly enhanced activity and stability compared to a single nickel. This finding can be attributed to the electronic effect exerted by the second metal which reduces onset potential.

#### 3.2.1. Alloying with Noble-Metal Nickel-Based Catalysts

Nickel-based materials alloyed with noble metals can effectively reduce the amount of precious metals required to maintain high performance for UOR. While earth-abundant inexpensive catalysts are presently used as anode materials for UOR and DUFC, catalytic activity still suffers from large-scale application. Low content noble metals and their alloys still possess extremely important research value. Kim et al. synthesized noble-metal- and nickel-based alloy carbon materials including Pd–Ni/C, Ag–Ni/C, and Pt–Ni/C via a co-sputtering method using a shadow mask (Figure 3A). After delicate tailoring, the Pd–Ni/C catalyst with a ratio of 60:40 showed the highest catalytic performance and stability [62]. Kim et al. synthesized nanocomposites of Ni/Pd-supported bead-carbonized nanofibers via electrospinning polyvinyl alcohol (PVA) followed by calcination under argon atmosphere (Figure 3B). These Ni/Pd-supported bead-carbonized nanofibers can substitute the costly precious metal (Pt) as they show high activity for UOR [80]. Wang et al. synthesized ultrathin NiFeRh–LDH nanosheets on the surface of NF via doping Rh into NiFe–LDH composites through the one-pot ethylene-glycol-assisting hydrothermal method. UOR electrocatalysis by NiFeRh–LDH nanosheets to achieve  $10 \text{ mA cm}^{-2}$  only requires 1.346 V (vs. RHE) in 1 M KOH with 0.33 M urea, and a constructed urine-mediated electrolysis cell needs a potential as low as 1.35 V to achieve  $10 \text{ mA cm}^{-2}$  (Figure 3C). Density functional theoretic (DFT) showed larger adsorption-free energy of urea on NiFeRh–LDH than on NiFe–LDH, indicating that rich oxygen vacancies of NiFeRh–LDH greatly improved UOR kinetics [81]. Wang et al. reported that in situ growth of low-Ir-content-doped Ni-based MOF ultrathin nanosheets on NF by the solvothermal method showed excellent performance in UOR. High-valence and low-content Ir cations incorporated into Ni–MOF structures can result in a more electrochemically active surface area, accelerated electron transfer, and chemical stability (Figure 3D). These advantages contribute to the highly efficient electrocatalytic performance of UOR, which achieves  $10 \text{ mA cm}^{-2}$  at 1.349 V in 1 M KOH with 0.5 M urea electrolytes and satisfactory stability [82]. Hong et al. synthesized 3D NiCo–LDH NSAs with  $\text{Ag}^0$  or  $\text{Au}^0$  and  $\text{Pd}^0$  intercalations by a hydrothermal treatment and liquid phase reduction via sodium borohydride. Improved activity in UOR can be attributed to heterostructures that contribute to the synergetic effect between support and doped nanoparticles [83].

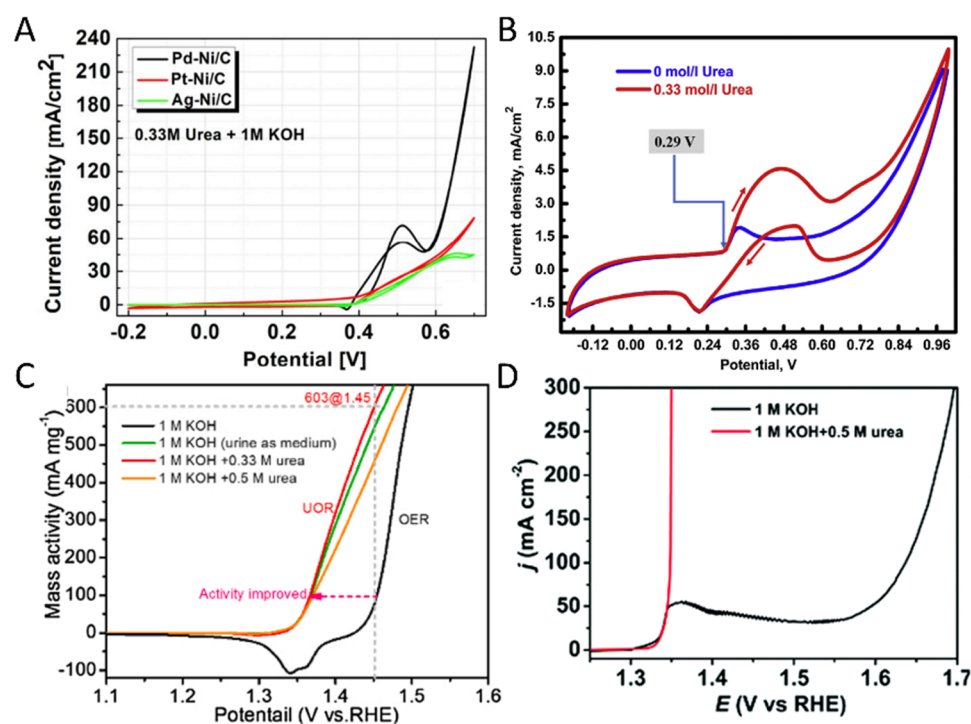


**Figure 3.** (A) CVs of the different electrodes in 1 mol L 1 KOH with urea [62]. Reproduced with permission [62]. Copyright 2019, Elsevier B.V. (B) Cyclic voltammetry of NFs in the presence and absence of 0.33 M urea in alkaline medium [80]. Reproduced with permission [80]. Copyright 2012, Elsevier B.V. (C) Mass normalized LSV curves of NiFeRh-LDH in N<sub>2</sub>-saturated 1 M KOH solution with or without urea or urine at 5 mV s<sup>-1</sup> [81]. Reproduced with permission [81]. Copyright 2020, Elsevier B.V. (D) LSV curves of NiIr-MOF/NF in 1 M KOH solution and with 0.5 M urea, respectively [82]. Reproduced with permission [82]. Copyright 2020, Wiley-VCH Verlag GmbH & Co. KGaA, Weinheim.

### 3.2.2. Alloying with Non-Noble-Metal Nickel-Based Catalysts

Nickel-based alloys especially with non-noble-metal materials have shown higher current density and lower oxidation potentials for UOR compared to single-metal nickel-based catalysts. Additionally, various novel nickel-based catalysts based on morphology modification have been developed; e.g., nickel nanoribbons [84], nickel-carbon sponges [85], nickel nanowires [86,87], and nickel nanoparticles [75]. Al-Deyab et al. synthesized NiMn nanoparticle-decorated carbon nanofibers through calcination, and electrospun mats composed with nickel and Mn ions and poly(vinyl alcohol) at 850 °C as effective electrocatalysts for UOR. The Mn-containing nanofibers distinctly enhanced electrocatalytic activity of UOR (Figure 4A). The electrochemical measurements indicated achievement of current densities of 300 mA cm<sup>-2</sup>g<sup>-1</sup> with an initial potential of 290 mV (vs. Ag/AgCl) [69]. Yoon et al. developed a novel free-standing Ni- and Cr-impregnated nanofiber by electrospinning polyacrylonitrile (Figure 4B). Further electrochemical measurements showed that 40% doping Cr-based NiCr<sub>4</sub>-CNT@C led to the best catalytic performance, achieving peak current densities of 145.5 mA cm<sup>-2</sup> at 0.62 V (vs. SCE) [78]. Xia et al. studied a bifunctional NiMo alloy nanotube for efficient hydrogen production as well as UOR via the hydrothermal and subsequent calcination process under Ar/H<sub>2</sub> atmosphere (Figure 4C). Benefiting from excellent metallicity and electronic structure, the Mo center was identified as the main activity site for urea chemisorption and O–H bond. The catalysts showed ultralow potentials of –44 mV and 1.36 V (vs. RHE) to achieve 10 mVcm<sup>-2</sup> [88]. Wei et al. designed a NiMo@ZnO/NF electrode with ZnO as the template and a core covered by NiMo alloys via electrodeposition. A 3D hierarchical NiMo alloy arrayed on nickel foam as a microrod for high-performance HER and UOR was a bifunctional catalyst which only required –110 mV and 1.405 V

to achieve  $10 \text{ mA cm}^{-2}$  towards HER and UOR, respectively [89]. Liu et al. designed bimetallic NiCo/Cr nanoparticle-encapsulated carbon nanofibers via electrospinning and carbonization. The trimetallic (CoNi/Cr) system showed the highest current density and the peak current density of  $21.34 \text{ mA cm}^{-2}$  [90]. Arandiyani et al. developed free-standing Ni–Co alloy nanowire arrays with strong adherence on the Ti substrate that act as current collectors using modified template-assisted electrodeposition. The as-obtained sample during optimized possesses showed low onset oxidation potential of  $0.372 \text{ V}$  (vs. Hg/HgO) and peak current density of  $322.82 \text{ mA cm}^{-2}$  [91]. Chen et al. proposed a novel nickel-iron alloy nanoparticle encapsulated by carbon spheres on 3D microporous nickel foam (NF) via direct carbonization of nickel-organic frameworks (Figure 4D). An ultrathin layer of nitrogen-doped carbon which encapsulated on NiFe alloy nanoparticles tightly attached 3D NF and alloyed, allowing electrolyte migration and diffusion into hollow carbon spheres and increasing the performance for UOR [92]. Liu et al. designed nitrogen-doped carbon sheets supporting Ni@NiO–Cu@CuO composites via calcination of Ni- or Cu-containing metal-organic frameworks as bifunctional hybrid electrocatalysts. Owing to the synergistic effects of electrochemical conductivity, heteroatom-doped carbon composites and highly active mixed metals with their oxide composites exhibited superior performance and stability for UNFC [93]. Schechter et al. synthesized Ni- and Sn-dendrite catalysts by direct electrodeposition of Ni on Sn-dendrite applications for UOR (Figure 4E). The as-obtained catalyst showed current densities of  $44 \text{ mA cm}^{-2}$  on  $0.55 \text{ V}$ , owing to the lower charge-transfer resistance in Ni and Sn dendrites [94].

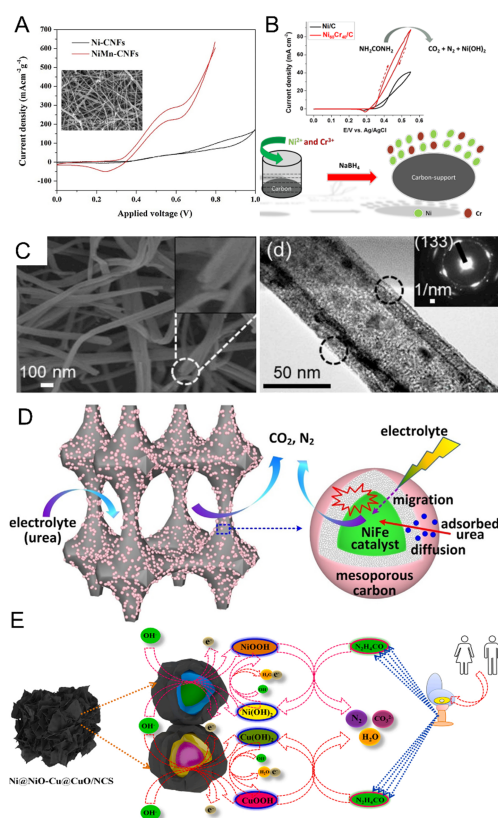


**Figure 4.** (A) Cyclic voltammograms for Ni–CNFs and NiMn–CNFs at 1.0 M urea concentration in 1.0 M KOH [69]. Reproduced with permission [69]. Copyright 2015, Elsevier B.V. (B) TOC of UOR on NiCr catalysts in alkaline electrolyte [78]. Reproduced with permission [78]. Copyright 2017, Wiley–VCH Verlag GmbH & Co. KGaA, Weinheim. (C) SEM and TEM images of NiMo nanotube [88]. Reproduced with permission [88]. Copyright 2019, Elsevier Ltd. (D) Illustration of enhanced UOR with CE–NiFe/NF electrode [92]. Reproduced with permission [92]. Copyright 2017, Elsevier Ltd. (E) UOR mechanism involved in Ni@NiO–Cu@CuO/NCS [94]. Reproduced with permission [94]. Copyright 2021, Elsevier B.V.

### 3.3. Heteroatom Modified Nickel-Based Catalysts

#### 3.3.1. Nickel-Based Chalcogenides

Chalcogen elements including O, S, Se, and Te with obvious metallic or non-metallic characteristics that have formed compounds with nickel elements are regarded as excellent candidates for UOR due to unique electron properties and good conductivity. Feng, et al. demonstrated a sample freeze-drying and annealing strategy to tune phase the structure of graphene, which supported Ni–NiO nanoparticle systems in efficiently boosting UOR performance (Figure 5A). The results showed that 450 °C was the best annealing temperature for performance since it increases the synergistic effect and conductivity of the Ni–NiO system [95]. Wang et al. fabricated Ni<sub>3</sub>S<sub>2</sub> nanowires directly grown on NF by one-step hydrothermal sulfurization. Ni<sub>3</sub>S<sub>2</sub>@NF displayed excellent catalytic activity for both UOR and HER in 1 M NaOH with 0.33 M urea; it achieved 100 mA cm<sup>-2</sup> and only need 360 mV overpotential [96]. Lu et al. proposed a unique strategy to control the synthesis of the different phases of NiTe on NF coated with GO. The electrocatalyst showed advanced activity at low potentials of 1.33 V for UOR in a mixed electrolyte of 1 M KOH and 0.33 M urea (Figure 5B). DFT calculations revealed the essential relationship between metallicity, ultrahigh conductivity of NiTe, and different binding interactions with CO<sub>2</sub> in UOR [89]. Li et al. successfully fabricated NiTe<sub>2</sub>/Ni(OH)<sub>2</sub> hybrid nanosheets via hydrothermal reaction on carbon fiber cloths (Figure 5C). The unique and strong electron synergistic interaction between NiTe<sub>2</sub> and Ni(OH)<sub>2</sub> led the as-fabricated catalyst to achieve 10 mA cm<sup>-2</sup> with a low overpotential of 73 mV for UOR in 1 M KOH with 0.33 M urea [97]. Wang et al. prepared a bifunctional electrocatalyst with NiCo–BDC nanosheet arrays that were covered by a thin film of Ni–S on NF substrates via a one-step hydrothermal process (Figure 5D). The as-obtained catalyst presented promising catalytic activity and stability for both OER and UOR, which reached a current density of 10 mA cm<sup>-2</sup> at a small potential of 1.31 V [98]. The secondary transition of metal into monometallic chalcogenides has been introduced as a strategy to tailor electronic and intermediate absorption energy to promote catalytic performance. Chen et al. developed self-supporting caterpillar spinal NiCo<sub>2</sub>S<sub>4</sub> arrays on nanosheet skeletons that were used to create trifunctional electrocatalysts for HER, OER, and UOR. The catalyst only needed 0.358 V vs. SCE to reach a current density of 50 mA cm<sup>-2</sup> for UOR [99]. Liu et al. designed 3D NiO/c-ESM nanocomposites using NiO immobilized in carbonized eggshell membranes through a two-step method. Carbonized 3D networks provide more catalyst surface area and activity sites, which enables wetting of the electrolyte and exhibits high selectivity and stability for UOR [100].

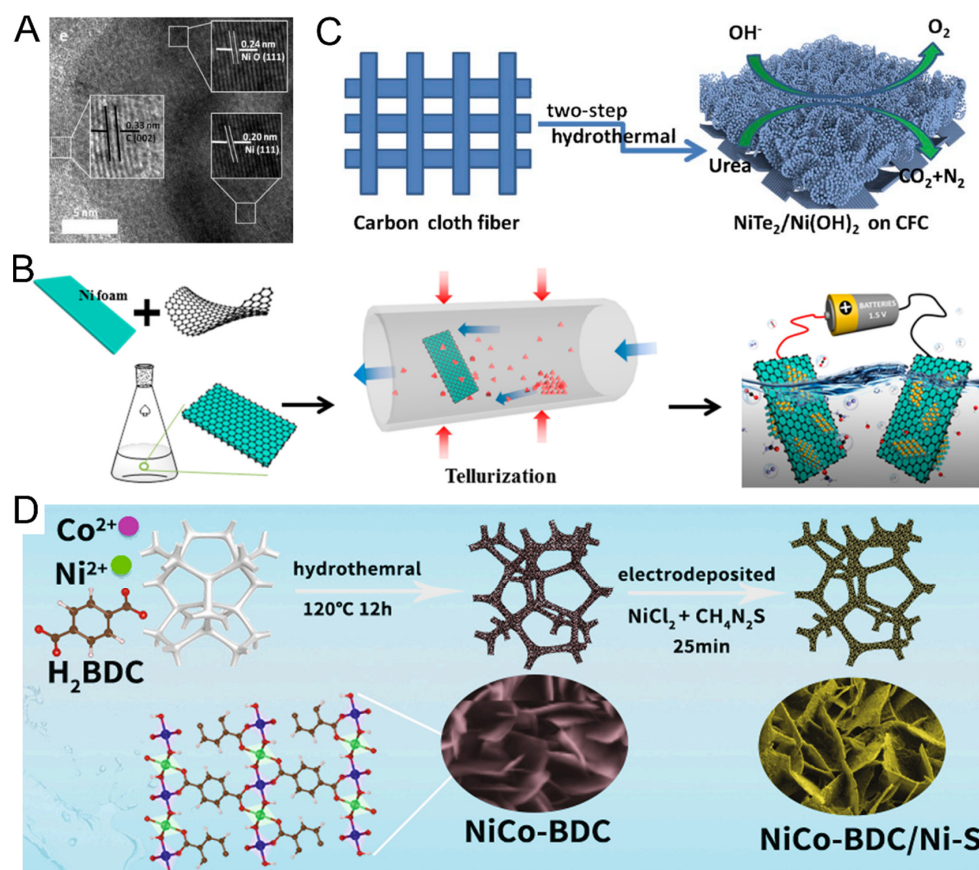


**Figure 5.** (A) TEM and HRTEM images of Ni-NiO/Gr-450 °C [95]. Reproduced with permission [95]. Copyright 2021, Elsevier Ltd. (B) Schematic illustration of synthesis processing of NiTe/rGO/NF [101]. Reproduced with permission [101]. Copyright 2019, American Chemical Society. (C) Schematic illustration of synthesis processing of hybrid NiTe<sub>2</sub>/Ni(OH)<sub>2</sub> nanosheets [97]. Reproduced with permission [97]. Copyright 2019, Elsevier B.V. (D) Schematic illustration of synthesis processing of NiCo-BDC/Ni-S nanosheets [98]. Reproduced with permission [98]. Copyright 2021, Elsevier B.V.

### 3.3.2. Nickel-Based Nitrogen-Element-Doped Compounds

Nitrogen element compounds with nickel, especially N and P, have extremely enhanced charge density states around the Fermi level which endows it with high electrical conductivity, beneficial for electrocatalytic processes in terms of electron transfer rate. Numerous efforts have been devoted for N- and P-based nickel compounds to modulate electronic structure and geometric effect to improve UOR electrocatalytic performance. Mei et al. demonstrated a novel bifunctional MOF-derived Ni<sub>3</sub>N, which firstly synthesizes Ni(OH)<sub>2</sub> on NF by hydrothermal reaction followed by calcination (Figure 6A). The 3D catalyst was shown to be highly active and durable for UOR, requiring 1.337 V to achieve 10 mA cm<sup>-2</sup> [102]. Sun et al. proposed a method using porous Ni<sub>3</sub>N nanosheet arrays on carbon cloths (CC), called Ni<sub>3</sub>N/CC, via nitridation with NH<sub>3</sub> from a Ni(OH)<sub>2</sub> nanoarray precursor on CC. Ni<sub>3</sub>N/CC exhibited high and durable performance for UOR and achieved 10 mA cm<sup>-2</sup> with only 1.35 V in 1 M KOH with 0.33 M urea [103]. Hong et al. developed carbon-doped hetero-structured Ni<sub>2</sub>P nanoparticles (named C@Ni<sub>2</sub>P) by a hydrothermal strategy and tailored by surface engineering of peapod-assisted nanorods and nanoparticles. C@Ni<sub>2</sub>P presented high performance for UOR in terms of current density and initial potential. These outcomes can be attributed to a higher surface area which leads to more accessible active centers and decreased blocking effect [104]. Cao et al. synthesized a porous Ni<sub>2</sub>P nanoflower which was supported on NF (Ni<sub>2</sub>P@Ni foam) by a hydrothermal method and phosphating strategy (Figure 6B). After delicately tailoring the catalyst structure, the

Ni<sub>2</sub>P@Ni foam reached peak current density of 750 mA cm<sup>-2</sup> with initial potential of 0.24 V (vs. Ag/AgCl) and superb stability in 0.60 M urea with 5.00 M KOH solutions [105].

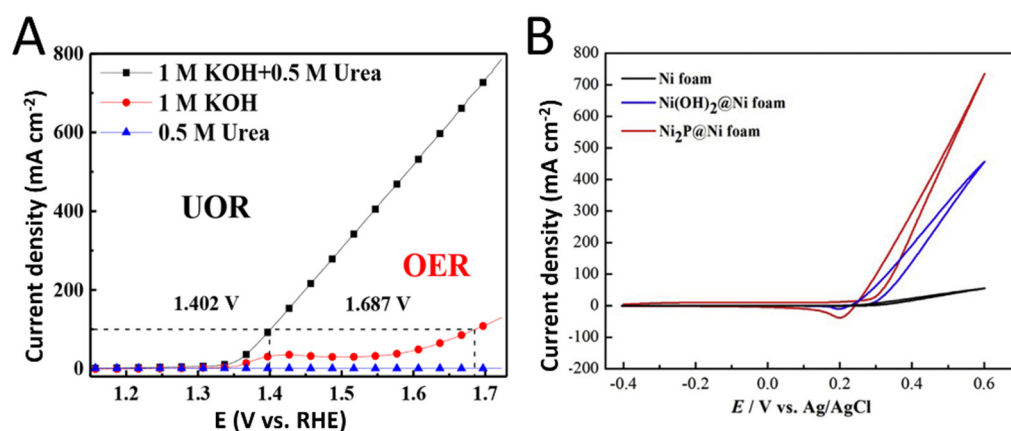


**Figure 6.** (A) LSVs of materials in 1.0 M KOH with 0.5 M urea [102]. Reproduced with permission [102]. Copyright 2020, American Chemical Society. (B) CVs of different electrodes in 5.00 M KOH solution with M urea [105]. Reproduced with permission [105]. Copyright 2018, Hydrogen energy Publication LLC. Published by Elsevier Ltd.

### 3.3.3. Nickel-Based Sulfides and Nitrogen-Dual-Doped Compounds

Nickel-based sulfides have been widely researched for UOR due to low cost, environment benignity, and high electrocatalytic activity. Nevertheless, poor electrical conductivity, low intrinsic activity, and less active site exposure restricted their widespread application. Incorporating nitrogen elements including N and P can efficiently tailor the electron structure of inner sulfides, influencing the catalyst structure and creating abundant active sites to enhance intrinsic activity. Feng et al. designed an activity catalyst by constructing nickel sulfides doped by N, simultaneously using amidino thiourea and thioacetamide as S and N sources for the catalyst fabrication process (Figure 7A). Benefiting from high activity, favorable kinetics, and rapid electron transfer leading to interfacial coupling and synergistic effect, the as-prepared N-doped NiS/NiS<sub>2</sub> achieved 100 mA cm<sup>-2</sup> at 1.47 V for UOR [106]. Sun et al. reported a novel bifunctional Ni<sub>2</sub>P/Ni<sub>0.96</sub>S microsphere cluster structure on nickel foam that was synthesized through two calcination steps (Figure 7B). The unique synergistic effect between Ni<sub>2</sub>P and Ni<sub>0.96</sub>S improved the performance of UOR and HER in terms of charge transfer resistance and number of exposed active sites, and we obtained 100 mA cm<sup>-2</sup> with a voltage of only 1.453 V, lower than those of 186 mV in 1 M KOH without 0.5 M urea [107]. Liu et al. designed growing coaxial Ni/NiS<sub>2</sub>- or Ni<sub>3</sub>S<sub>2</sub>@N-doped carbon nanofibers on NF as free-standing electrodes that presynthesized amorphous Ni<sub>3</sub>S<sub>2</sub>-coated N-doped nanofibers and crystalline Ni<sub>3</sub>S<sub>2</sub> nanoparticle shells by annealing in Ar. The metallic Ni nanoparticles were integrated into the shell during the annealing process which mixed Ar/H<sub>2</sub> into Ar gas under high temperatures (Figure 7C). The as-obtained electrodes displayed efficient HER and UOR performance, serving as the anode and cathode, respectively. The synthesized catalysts delivered a high current density of 20 mA cm<sup>-2</sup> at 1.5 V, outperforming most previously researched electrocatalysts for urea electrolysis [108].

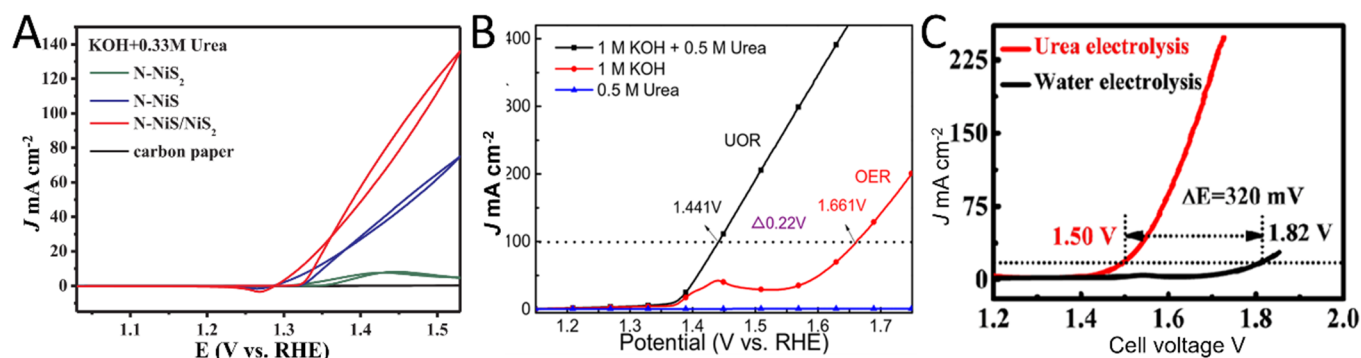


**Figure 7.** (A) UOR performance of sample in 1 M KOH with 0.33 M urea [106]. Reproduced with permission [106]. Copyright 2020, Elsevier B.V. (B) UOR curves of MS-Ni<sub>2</sub>P/Ni<sub>0.96</sub>S/NF in 1.0 M KOH with 0.5 M urea [107]. Reproduced with permission [107]. Copyright 2020, American Chemical Society. (C) Comparison of polarization curves of UOR and water splitting when using NF/PPy700Ni<sub>3</sub>S<sub>2</sub>-8-Ar as the anode and NF/PPy700Ni<sub>3</sub>S<sub>2</sub>-8-H<sub>2</sub> as the cathode in a two-electrode system [108]. Reproduced with permission [108]. Copyright 2021, American Chemical Society.

### 3.3.4. Heteroatom-Doped Nickel-Based Metal Compounds

Constructing nickel-based sulfide, oxide, and nitride hybrid nanostructures with other non-noble transition metals can effectively synergize their strengths to achieve superior activity and stability for UOR. Hou et al. reported a 3D hybrid nanostructure supported on NF, which was prepared by two-step calcination at 800 °C via immersion in an ammonium tetrathiomolybdate solution and at 400 °C in an ammonia atmosphere. The N-MoO<sub>2</sub>/Ni<sub>3</sub>S<sub>2</sub> hybrid with a particle grown on NF showed high activity and robust durability for both HER and UOR, achieving 100 mA cm<sup>-2</sup> with only 2.08 V, as well as a high biomass conversion ratio over 90% [109]. (Figure 8A) Yu et al. synthesized two types of nickel-molybdenum-based nanocomposite catalysts, i.e., NiMoO-Ar and NiMoO-H<sub>2</sub>, for high efficiency and performance in HER and UOR, fabricated via a gas-selected calcination process using NiMoO<sub>4</sub>·xH<sub>2</sub>O nanorods as precursors and model materials. An electrolyte composed of NiMoO-Ar and NiMoO-H<sub>2</sub> as anode and cathode achieved a current density of 10 mA cm<sup>-2</sup> with only 1.38 V and showed higher stability than the current best noble-metal-free electrocatalysts [1]. Shi et al. successfully prepared lantern-like porous and hollow NiO and Ni<sub>0.9</sub>Fe<sub>0.1</sub>O<sub>x</sub> microspheres composed of 2D nanosheets with ultrahigh SSA and ECSA using a coprecipitation strategy (Figure 8B). The as-obtained catalysts showed excellent catalytic activity for both HER and UOR and reached a current density of 10 mA cm<sup>-2</sup> while only requiring 1.455 V for overall urea splitting [110]. Cao et al. successfully constructed in situ vertical growth of thorny leaf-like NiCoP on CC (2D nanosheets supported by 1D nanowires named NiCoP/CC) as highly efficient bifunctional electrocatalysts (Figure 8C). Because of the unique hierarchical structure composed of 1D nanowires, 2D nanosheets, and 3D CC substrate as well as the synergistic effect between Ni and Co, the electrocatalyst showed excellent performance for both HER and UOR, with a current density of 10 mA cm<sup>-2</sup> at 1.42 V when used as the cathode and anode for overall urea splitting electrolyte [111]. Liu et al. provided a method that achieved a partial substitution of S in NiMoO<sub>4</sub> on NF (Figure 8D). Results of the electrocatalytic measurement and theoretical analysis showed that the electronic structure was extremely induced by S around density states near the E<sub>F</sub>, which optimized the NiMoO<sub>3</sub>S/NF catalyst and displayed better inherent kinetics as well as high catalytic activity [112]. Shahrokhian et al. synthesized flower-like structures (Ni<sub>x</sub>Co<sub>2-x</sub>P/C) in developing an MOF-carbon-based composite (Figure 8E). The authors utilized in situ emulsion polymerization of the mixture of aniline and pyrrole in the presence of Triton X-100 and followed with a carbonization process. Owing to the unique and novel electrocatalysts comprising 3D nanostructures, eNi<sub>x</sub>Co<sub>2-x</sub>P/C@HCNs only needed 1.33 V to achieve 10 mA cm<sup>-2</sup> in 1 M KOH containing 0.33 M urea [113]. Wen et al. designed and synthesized hybrid nanostructures composed

of nitrogen-doped carbon sheets via direct annealing of Cu- and Ni-containing metal organic frameworks (MOFs). The as-synthesized nanohybrid showed excellent electrocatalytic activity for both UOR and nitrate reduction reaction (NRR) in alkali and acidic electrolytes, and urea-nitrate fuel cells (UNFCs) exhibited improved fuel cell performance of  $22.55 \pm 2.3 \text{ mW cm}^{-2}$  for both the cathode and anode [93]. Lei et al. designed and successfully prepared 3D hierarchical  $\text{Ni}_4\text{N}/\text{Cu}_3\text{N}$  nanotube array structures on copper foam (CF) that exhibited excellent performance for both HER and UOR and achieved a current density of  $10 \text{ mA cm}^{-2}$  on  $-0.098 \text{ V}$  and  $1.34 \text{ V}$ , respectively. The high activity could be attributed to high morphologic and electrochemical characterization of metal nitrides and the unique hierarchical nanoarray structure [114]. Wang et al. prepared a highly activated  $\text{NiCo}_2\text{S}_4$  phase with novel nanosheet array topology structures on CC (noted as  $\text{NiCo}_2\text{S}_4\text{NS}/\text{CC}$ ) via traditional wet-chemistry sulfurization (anion exchange) of the precursor ( $\text{NiCo}_2\text{O}_4$ ). The flexible and versatile electrocatalyst showed high performance for both HER and UOR, and only needed  $1.66 \text{ V}$  and  $1.49 \text{ V}$  to achieve  $10 \text{ mA cm}^{-2}$  for overall water splitting and UOR [115].

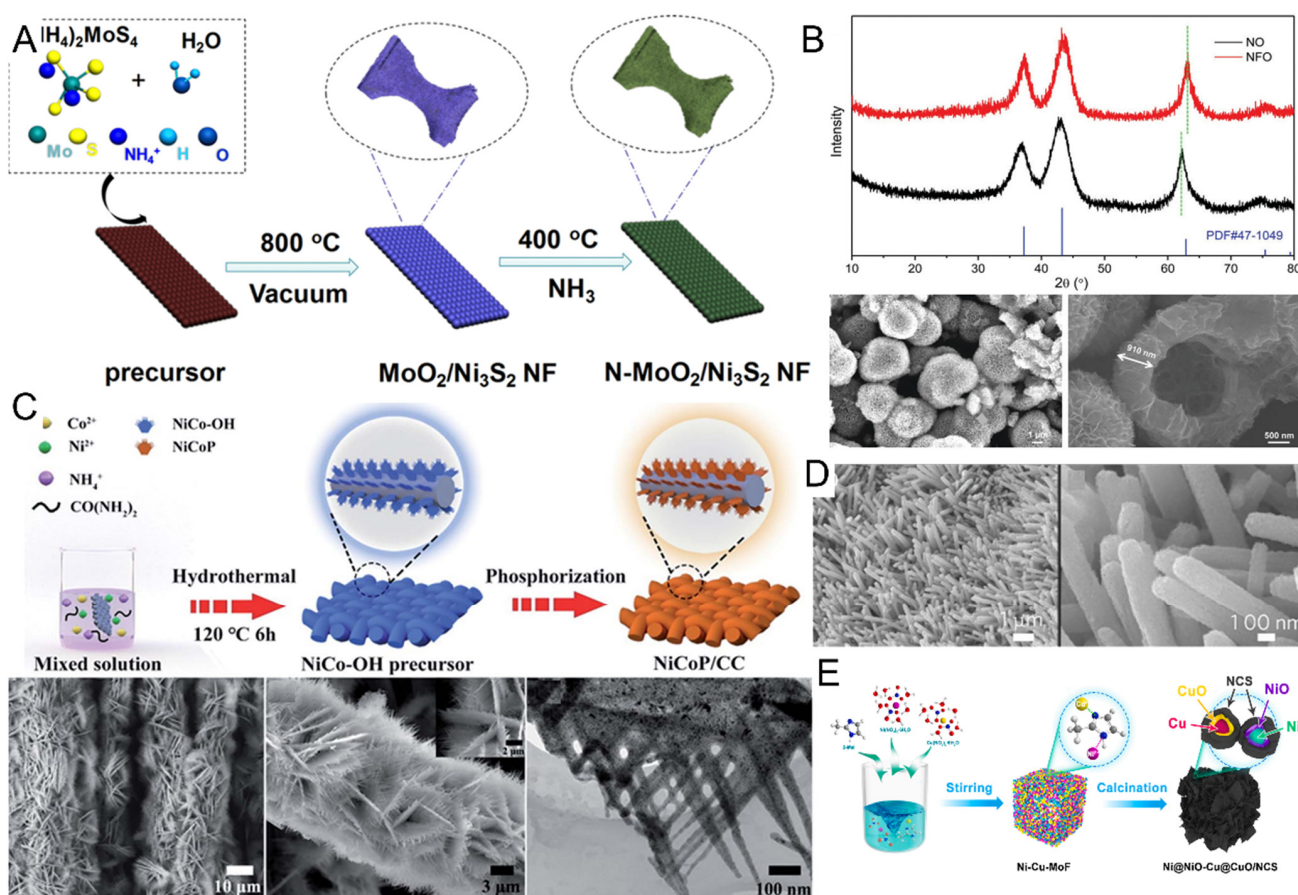


**Figure 8.** (A) Illustration of the synthesis process of  $\text{N-MoO}_2/\text{Ni}_3\text{S}_2\text{NF}$  [109]. Reproduced with permission [109]. Copyright 2019, American Chemical Society. (B) XRD pattern and SEM images of NFO powders [110]. Reproduced with permission [110]. Copyright 1996, Royal Society of Chemistry. (C) Schematic illustration of the fabrication process and low-high-magnification SEM and TEM images of the  $\text{NiCoP}/\text{CC}$  electrode [111]. Reproduced with permission [111]. Copyright 2013, Royal Society of Chemistry. (D) Low-high-magnification SEM images of the  $\text{NiMoO}_3\text{S}/\text{NF}$  electrode [112]. Reproduced with permission [112]. Copyright 1996, Royal Society of Chemistry. (E) Schematic illustration of the experimental design of  $\text{Ni@NiO-Cu@CuO}/\text{NCS}$  [93]. Reproduced with permission [93]. Copyright 2021, Elsevier B.V.

### 3.4. Nickel-Based Materials Compound with Carbon-Based Materials

The different substrates combined with nickel-based materials can significantly change the physical composition of catalysts and affect the physicochemical properties and catalytic activity. Carbon-based materials including carbon nanotube, active carbon, graphene and graphite, biomass carbon, and carbonaceous materials can significantly enhance the conductivity, rate of charge, and mass transfer and dispersion, and have been widespread applied to support catalysts in electrocatalysis. Nickel-based materials are widely compounded with the above carbon materials as one of the methods to improve catalytic activity of UOR via enhancing dispersion and conductivity. Yang et al. synthesized a tungsten carbide- and cobalt-modified Ni-based catalyst (MWCNTs) via an impregnation method for UOR. In this study, multiwall carbon nanotubes enhanced conductivity and dispersion which simultaneously improved and reduced the current density and overpotential, respectively [116]. Wang et al. synthesized a series of multivariate MOFs based on  $\text{Zn}^{2+}/\text{Ni}^{2+}$  and 1,3,5-trimesic acid (BTC) by tuning the ration of Zn/Ni and solvothermal method (Figure 9A). The materials were thoroughly characterized by XRD and XPS which confirmed the existence of Ni metal and NiO. Owing to the highly porous pomegranate-like Ni/C-1 that is derived from Zn/Ni-BTC under the Zn/Ni atom ration of 1, the catalyst exhibited superb HER performance and a small onset potential of 1.33 V vs RHE in 1 M KOH [117]. Yang et al. designed active nickel nanoparticles embedded into nitrogen-doped carbon nanotubes (named Ni@NCNT) via carbonization of the nickel precursor and dicyandiamide in the nitrogen atmosphere as an efficient and stable UOR electrocatalyst (Figure 9C). Due to the unique structure of N-doped carbon and Ni nanoparticles for wetting electrolytes and facilitating metallic Ni electrochemical conversion to active  $\text{Ni}^{3+}$  species leading to a robust UOR activity, the well configuration of N atom electronic structures in modulation of catalytic activity weaken the binding strength between generated  $\text{CO}_2$  species and adjacent active sites to accelerate the  $\text{CO}_2$  adsorption. As a result, the as-fabricated materials only need 1.5 V vs. RHE to achieve a current density of  $45.8 \text{ mA cm}^{-2}$ , which is 3.8 times better than commercial Pt/C in 1 M KOH with 0.5 M urea electrolyte [118]. Sathe et al. proposed an effective strategy to decorate Ni nanoparticles on GO via a chemical reduction method and characterize them by infrared spectroscopy (IR), X-ray diffraction (XRD), transmission electron microscopy (TEM), etc. Structural and morphological studies confirm the particle size of Ni NPs (10 nm) and thickness of GO (20 nm) (Figure 9B). Benefitting from the large active area which creates an easy path for electron and mass transfer and electronic support of Ni species, Ni@GO enhanced the electrocatalytic activity compared to individual counterparts (e.g., Ni NPs and GO) [119].

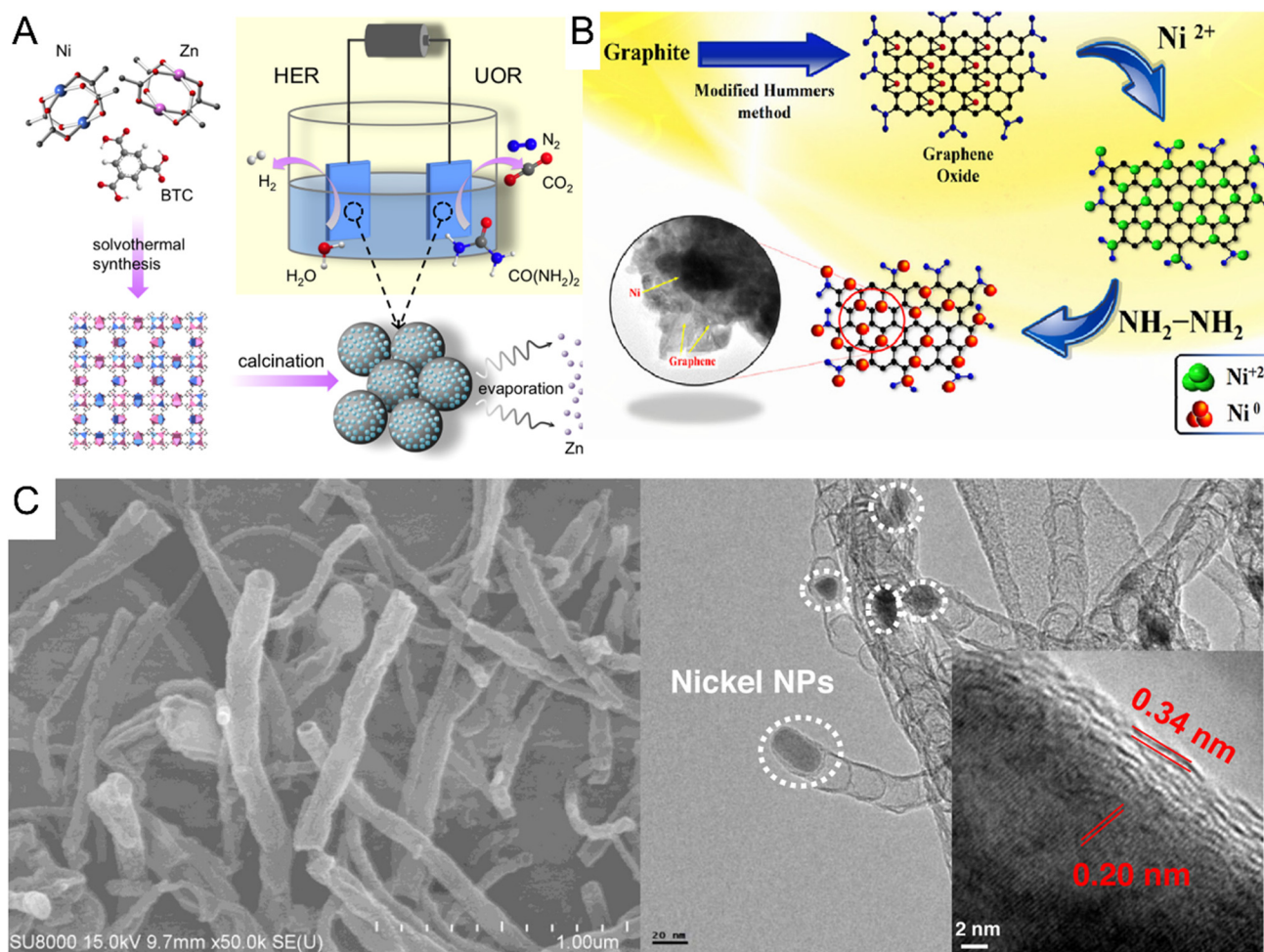


**Figure 9.** (A) Schematic representation of the synthesis and bifunctionality of Ni/C composite [117]. Reproduced with permission [117]. Copyright 2018, American Chemical Society. (B) SEM, TEM, and HAADF-STEM of Ni@NCNT [118]. Reproduced with permission [118]. Copyright 2020, Elsevier B.V. (C) Schematic for synthesis of Ni@GO nanomaterials [119]. Reproduced with permission [119]. Copyright 2020, Elsevier Ltd.

### 3.5. Others Structural Modifications of Nickel-Based Materials

Other modifications of nickel-based materials occur on macro and micro levels such as oxygen vacancy, Schottky heterojunction, and nickel vacancy and have important influences in the electrocatalytic field and understanding the underlying correlations between microstructures and intrinsic UOR activity. Peng et al. proposed a lattice-oxygen-involved UOR mechanism on  $\text{Ni}^{4+}$  which has more favorable reaction kinetics than conventional UOR mechanisms. In accordance with DFT, in situ IR spectroscopy, mass spectroscopy, and performance testing,  $^{18}\text{O}$  isotope-labeling is directly involved in UOR, which could transfer  $\text{CO}^*$  to  $\text{CO}_2$  and accelerate the reaction rate. Finally, the resulting catalyst containing  $\text{Ni}^{4+}$  exhibits a high current density of  $264 \text{ mA cm}^{-2}$  at 1.6 V vs. RHE on a glassy carbon electrode, outperforming the state-of-the-art catalysts for UOR by five times [120]. Wang et al. proposed that metals and semiconductors can combine through phases to form the Mott-Schottky heterojunction, which promotes non-precious-metal catalysts for UOR activities. According to the above concept, the author designed a Mott-Schottky catalyst through an electrochemical reduction converting the semiconductor  $\text{CoMn}_2\text{O}_4$  to metallic CoMn. The catalyst enhanced metallicity and electron redistribution, reduced reaction barriers, and promoted the breaking of chemical bonds in UOR processing, which finally exhibited superior catalytic activity that achieved a  $100 \text{ mA cm}^{-2}$  current density with

only 1.36 V vs. RHE, as well as excellent stability [121]. Song et al. developed various nickel hydroxide ( $\alpha$ -Ni(OH)<sub>2</sub>) samples with adjustable nickel vacancy concentrations by an electrochemical reconstruction method to comprehensively understand the correlation between intrinsic structure and catalytic mechanisms (Figure 10A). Based on DFT and experimental measurements, the reconstruction of  $\alpha$ -Ni(OH)<sub>2</sub> showed that the introduction of  $V_{Ni}$ -enhanced intrinsic conductivities and thereby improved activities for UOR [122]. Xie et al. fabricated oxygen-vacancy-rich NiMoO<sub>4</sub> through a defect engineering strategy using a top-down hydrothermal method on NF (Figure 10B). Experimental and DFT results further confirmed that O-vacancies rich in NiMoO<sub>4</sub> can have synergetic effects with higher exposed active sites, faster electron and mass transformation, and low reaction barriers of UOR processing, significantly enhancing electrocatalytic activity [123].

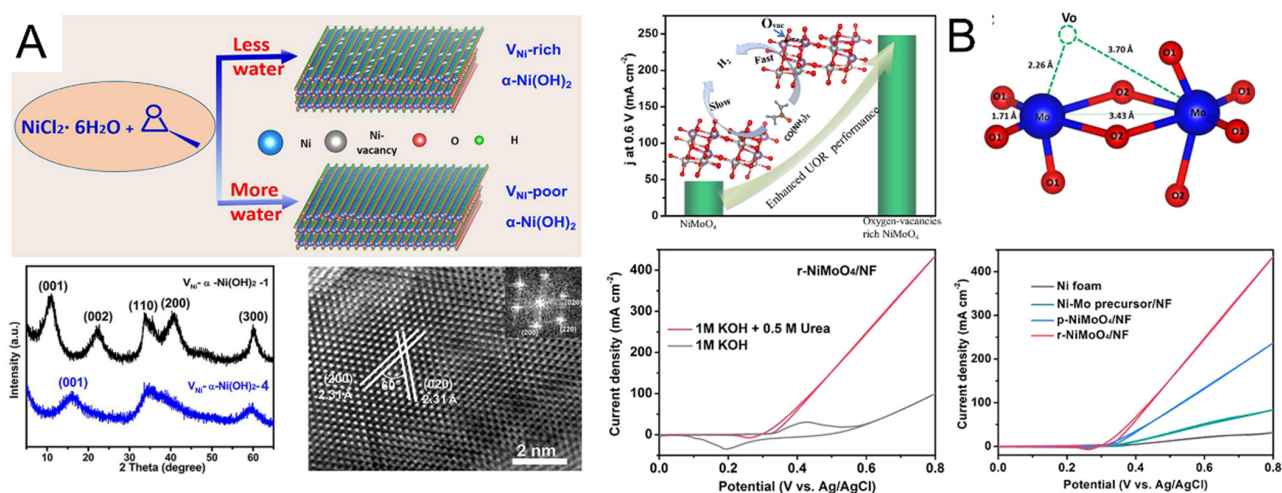


**Figure 10.** (A) Schematic diagram of the synthesis of  $V_{Ni}$   $\alpha$ -Ni(OH)<sub>2</sub> and typical XRD with HRTEM characterization of materials [122]. Reproduced with permission [122]. Copyright 2018, American Chemical Society. (B) Experimental and DFT results of as-prepared samples [123]. Reproduced with permission [123]. Copyright 2018, American Chemical Society.

#### 4. Conclusions and Perspectives

The extensive use of urea has made important contributions to the development and progress of modern human society. Along with this is pollution of water and soil that also greatly affects the normal ecological environment. Much of urea in the urine of human and animal excretes in the natural environment further deteriorate of the local environment, and the amount of urea present directly affects human health. Therefore, it is of great significance to effectively purify urea-rich wastewater and improve the detection of human health. Among the many detection strategies, electrochemical oxidation is one of the most effective methods that is fast, easy, extremely selective, and easy to operate. Many research studies report that nickel-based catalysts have been considered as the most effective energy utilization and strategy to enhance detection and treatment for UOR. In this review, we summarized the types of nickel-based catalysts and the main methods and mechanisms of catalysts in structure and design. To advance the research on technologies and nickel-based catalysts for UOR, the following are several foreseeable challenges and research directions:

- (1) The formation of alloys including noble metals and non-noble metals allows changes the microstructure of materials which significantly improves the activity and stability of the catalyst;
- (2) Nickel-based layered double hydroxide compounds with other metals and nanostructures through intercalation and modification can effectively improve conductivity and increase the number of edge active sites;

(3) The negative charge of sulfur group elements (O, S, Se, and Te) can effectively change the charge distribution of nickel metals and enhance the adsorption and desorption of reactive intermediates in UOR, enhancing catalytic activity;

(4) Complexing with nitrogen group elements (mainly the unique electronic properties of N and P) changes the Fermi energy level window and electron geometry distribution of the materials, improving conductivity of the materials and promoting activity;

(5) Various carbon material composites with nickel-based materials can effectively improve dispersion on the nanoscale, improving the conductivity, electron and mass transfer capacity, and catalytic activity; and

(6) Various structural designs such as oxygen vacancy, Schottky heterojunction, nickel-based vacancy, and defect-rich structure can help deeply understand and modify materials from an atomic nucleus microstructure perspective.

Until now, despite encouraging progress in the development of high-efficiency nickel-based UOR catalysts and the continual accumulation of experimental data in this field to understand fundamental catalytic mechanisms and processes, the field still faces severe challenges in terms of practical operation and cost-effectiveness. On one hand, more and more in situ characterizations and theoretical studies continue to reveal details of reaction steps and intermediates. On the other hand, it also requires researchers to collaborate with industries to advance the performance of catalysts in electrolytic cells and fuel cells. We believe that the introduction of novel and promising catalyst supports contributes to improving the conductivity, stability, and electrochemical activity of catalysts for urea splitting and DUFC, as well as creating more sustainable and cost-effective technologies that can be used in such energy conversion systems for sewage treatment and urea detection and conversion.

**Funding:** This study was supported by the Xi'an Municipal Bureau of Science and Technology (201805056ZD7CG40), the National Natural Science Foundation of China (21405119), and the Natural Science Basic Research Plan in Shaanxi Province of China (2015JQ2046).

**Acknowledgments:** Ma (Yaming) and Chenxiang are responsible for the conception and writing of the manuscript. Yingche Wang and Ke Wang are responsible for the data analysis, modification and finalization of the manuscript.

**Conflicts of Interest:** The authors declare no conflict of interest.

## References

1. Yu, Z.-Y.; Lang, C.-C.; Gao, M.-R.; Chen, Y.; Fu, Q.-Q.; Duan, Y.; Yu, S.-H. Ni–Mo–O nanorod-derived composite catalysts for efficient alkaline water-to-hydrogen conversion via urea electrolysis. *Energy Environ. Sci.* **2018**, *11*, 1890–1897. [[CrossRef](#)]
2. Keshet, R.; Szlosarek, P.; Carracedo, A.; Erez, A. Rewiring urea cycle metabolism in cancer to support anabolism. *Nat. Rev. Cancer* **2018**, *18*, 634–645. [[CrossRef](#)] [[PubMed](#)]
3. Meng, F.; Seredych, M.; Chen, C.; Gura, V.; Mikhalovsky, S.; Sandeman, S.; Ingavle, G.; Ozulumba, T.; Miao, L.; Anasori, B.; et al. MXene sorbents for removal of urea from dialysate: A step toward the wearable artificial kidney. *ACS Nano* **2018**, *12*, 10518–10528. [[CrossRef](#)]
4. Batshaw, M.L.; Brusilow, S.; Waber, L.; Blom, W.; Brubakk, A.M.; Burton, B.K.; Cann, H.M.; Kerr, D.; Mamunes, P.; Matalon, R.; et al. Treatment of inborn errors of urea synthesis—activation of alternative pathways of waste nitrogen synthesis and excretion. *N. Engl. J. Med.* **1982**, *306*, 1387–1392. [[CrossRef](#)] [[PubMed](#)]
5. Chen, C.; Zhu, X.; Wen, X.; Zhou, Y.; Zhou, L.; Li, H.; Tao, L.; Li, Q.; Du, S.; Liu, T.; et al. Coupling N<sub>2</sub> and CO<sub>2</sub> in H<sub>2</sub>O to synthesize urea under ambient conditions. *Nat. Chem.* **2020**, *12*, 717–724. [[CrossRef](#)] [[PubMed](#)]
6. Lee, J.S.; Adler, L.; Karathia, H.; Carmel, N.; Rabinovich, S.; Auslander, N.; Keshet, R.; Stettner, N.; Silberman, A.; Agemy, L.; et al. Urea Cycle Dysregulation Generates Clinically Relevant Genomic and Biochemical Signatures. *Cell* **2018**, *174*, 1559–1570.e22. [[CrossRef](#)]
7. Wang, G.; Ling, Y.; Lu, X.; Wang, H.; Qian, F.; Tong, Y.; Li, Y. Solar driven hydrogen releasing from urea and human urine. *Energy Environ. Sci.* **2012**, *5*, 8215. [[CrossRef](#)]
8. Zhang, Z.; Chen, X.; Zhang, H.; Liu, W.; Zhu, W.; Zhu, Y. A highly crystalline perylene imide polymer with the robust built-in electric field for efficient photocatalytic water oxidation. *Adv. Mater.* **2020**, *32*, e1907746. [[CrossRef](#)]
9. Shukla, K.; Srivastava, V.C. Synthesis of organic carbonates from alcoholysis of urea: A review. *Catal. Rev.* **2017**, *59*, 1–43. [[CrossRef](#)]

10. Forslund, R.P.; Mefford, J.T.; Hardin, W.G.; Alexander, C.T.; Johnston, K.P.; Stevenson, K.J. Nanostructured LaNiO<sub>3</sub> perovskite electrocatalyst for enhanced urea oxidation. *ACS Catal.* **2016**, *6*, 5044–5051. [[CrossRef](#)]
11. Van Gelder, M.K.; Jong, J.A.W.; Folkertsma, L.; Guo, Y.; Bluchel, C.; Verhaar, M.C.; Odijk, M.; Van Nostrum, C.F.; Hennink, W.E.; Gerritsen, K.G.F. Urea removal strategies for dialysate regeneration in a wearable artificial kidney. *Biomaterials* **2020**, *234*, 119735. [[CrossRef](#)] [[PubMed](#)]
12. An, X.; Stelter, D.; Keyes, T.; Reinhard, B.M. Plasmonic Photocatalysis of urea oxidation and visible-light fuel cells. *Chem* **2019**, *5*, 2228–2242. [[CrossRef](#)]
13. Li, C.; Liu, Y.; Zhuo, Z.; Ju, H.; Li, D.; Guo, Y.; Wu, X.; Li, H.; Zhai, T. Local Charge Distribution Engineered by Schottky Heterojunctions toward Urea Electrolysis. *Adv. Energy Mater.* **2018**, *8*, 1801775. [[CrossRef](#)]
14. Krajewska, B. Ureasases I. Functional, catalytic and kinetic properties: A review. *J. Mol. Catal. B Enzym.* **2009**, *59*, 9–21. [[CrossRef](#)]
15. Xue, C.; Wilson, L.D. Kinetic study on urea uptake with chitosan based sorbent materials. *Carbohydr. Polym.* **2016**, *135*, 180–186. [[CrossRef](#)]
16. Liu, X.; Sun, S.; Tang, Y.; Li, S.; Chang, J.; Guo, L.A.; Zhao, Y. Preparation and kinetic modeling of cross-linked chitosan microspheres immobilized Zn(II) for urea adsorption. *Anal. Lett.* **2012**, *45*, 1632–1644. [[CrossRef](#)]
17. Zhu, L.-J.; Liu, F.; Yu, X.-M.; Gao, A.-L.; Xue, L.-X. Surface zwitterionization of hemocompatible poly(lactic acid) membranes for hemodiafiltration. *J. Membr. Sci.* **2015**, *475*, 469–479. [[CrossRef](#)]
18. Simka, W.; Piotrowski, J.; Robak, A.; Nawrat, G. Electrochemical treatment of aqueous solutions containing urea. *J. Appl. Electrochem.* **2009**, *39*, 1137–1143. [[CrossRef](#)]
19. Mahalik, K.; Sahu, J.N.; Patwardhan, A.V.; Meikap, B.C. Kinetic studies on hydrolysis of urea in a semi-batch reactor at atmospheric pressure for safe use of ammonia in a power plant for flue gas conditioning. *J. Hazard. Mater.* **2010**, *175*, 629–637. [[CrossRef](#)]
20. Von Ahnen, M.; Pedersen, L.-F.; Pedersen, P.B.; Dalsgaard, J. Degradation of urea, ammonia and nitrite in moving bed biofilters operated at different feed loadings. *Aquac. Eng.* **2015**, *69*, 50–59. [[CrossRef](#)]
21. Ieropoulos, I.; Greenman, J.; Melhuish, C. Urine utilisation by microbial fuel cells; energy fuel for the future. *Phys. Chem. Chem. Phys.* **2012**, *14*, 94–98. [[CrossRef](#)] [[PubMed](#)]
22. Ananiev, A. The urea decomposition in the process of the heterogeneous catalytic denitration of nitric acid solutions Part I. Kinetics of the reaction. *Appl. Catal. B Environ.* **2003**, *45*, 189–196. [[CrossRef](#)]
23. Shen, S.; Li, M.; Li, B.; Zhao, Z. Catalytic hydrolysis of urea from wastewater using different aluminas by a fixed bed reactor. *Environ. Sci. Pollut. Res. Int.* **2014**, *21*, 12563–12568. [[CrossRef](#)]
24. Lundström, A.; Snelling, T.; Morsing, P.; Gabriëlsson, P.; Senar, E.; Olsson, L. Urea decomposition and HNCO hydrolysis studied over titanium dioxide, Fe-Beta and  $\gamma$ -Alumina. *Appl. Catal. B Environ.* **2011**, *106*, 273–279. [[CrossRef](#)]
25. Xu, H.; Ye, K.; Zhu, K.; Yin, J.; Yan, J.; Wang, G.; Cao, D. Template-directed assembly of urchin-like CoS<sub>x</sub>/Co-MOF as an efficient bifunctional electrocatalyst for overall water and urea electrolysis. *Inorg. Chem. Front.* **2020**, *7*, 2602–2610. [[CrossRef](#)]
26. Jiang, Y.; Gao, S.; Liu, J.; Xu, G.; Jia, Q.; Chen, F.; Song, X. Ti-Mesh supported porous CoS<sub>2</sub> nanosheet self-interconnected networks with high oxidation states for efficient hydrogen production via urea electrolysis. *Nanoscale* **2020**, *12*, 11573–11581. [[CrossRef](#)]
27. Singh, T.I.; Rajeshkhanna, G.; Singh, S.B.; Kshetri, T.; Kim, N.H.; Lee, J.H. Metal-Organic Framework-derived Fe/Co-based Bifunctional electrode for H<sub>2</sub> production through water and urea electrolysis. *ChemSusChem* **2019**, *12*, 4810–4823. [[CrossRef](#)] [[PubMed](#)]
28. Omer, A.M. Energy, environment and sustainable development. *Renew. Sustain. Energy Rev.* **2008**, *12*, 2265–2300. [[CrossRef](#)]
29. Satyapal, S.; Petrovic, J.; Read, C.; Thomas, G.; Ordaz, G. The U.S. Department of Energy's National Hydrogen Storage Project: Progress towards meeting hydrogen-powered vehicle requirements. *Catal. Today* **2007**, *120*, 246–256. [[CrossRef](#)]
30. Aroonratsameruang, P.; Pattanasattayavong, P.; Dorcet, V.; Mériadec, C.; Ababou-Girard, S.; Fryars, S.; Loget, G. Structure–property relationships in redox-derivatized metal–insulator–semiconductor (MIS) Photoanodes. *J. Phys. Chem. C* **2020**, *124*, 25907–25916. [[CrossRef](#)]
31. Liu, J.; Li, J.; Shao, M.; Wei, M. Directed synthesis of SnO<sub>2</sub>@BiVO<sub>4</sub>/Co-Pi photoanode for highly efficient photoelectrochemical water splitting and urea oxidation. *J. Mater. Chem. A* **2019**, *7*, 6327–6336. [[CrossRef](#)]
32. Loget, G.; Meriadec, C.; Dorcet, V.; Fabre, B.; Vacher, A.; Fryars, S.; Ababou-Girard, S. Tailoring the photoelectrochemistry of catalytic metal-insulator-semiconductor (MIS) photoanodes by a dissolution method. *Nat. Commun.* **2019**, *10*, 3522. [[CrossRef](#)] [[PubMed](#)]
33. Zhang, J.J.; Bao, W.W.; Li, M.Y.; Yang, C.M.; Zhang, N.N. Ultrafast formation of an FeOOH electrocatalyst on Ni for efficient alkaline water and urea oxidation. *Chem. Commun.* **2020**, *56*, 14713–14716. [[CrossRef](#)] [[PubMed](#)]
34. Song, M.; Zhang, Z.; Li, Q.; Jin, W.; Wu, Z.; Fu, G.; Liu, X. Ni-foam supported Co(OH)F and Co-P nanoarrays for energy-efficient hydrogen production via urea electrolysis. *J. Mater. Chem. A* **2019**, *7*, 3697–3703. [[CrossRef](#)]
35. Sun, Y.; Wang, S.; Ning, J.; Zhang, Z.; Zhong, Y.; Hu, Y. A one-pot “shielding-to-etching” strategy to synthesize amorphous MoS<sub>2</sub> modified CoS/Co<sub>0.85</sub>Se heterostructured nanotube arrays for boosted energy-saving H<sub>2</sub> generation. *Nanoscale* **2020**, *12*, 991–1001. [[CrossRef](#)]
36. Ghouri, Z.K.; Elsaïd, K.; Al-Meer, S.; Barakat, N.A.M. Applicable anode based on Co<sub>3</sub>O<sub>4</sub>–SrCO<sub>3</sub> heterostructure nanorods-incorporated CNFs with low-onset potential for DUFCS. *Appl. Nanosci.* **2017**, *7*, 625–631. [[CrossRef](#)]

37. Xu, Y.; Ren, T.; Ren, K.; Yu, S.; Liu, M.; Wang, Z.; Li, X.; Wang, L.; Wang, H. Metal-organic frameworks-derived Ru-doped Co<sub>2</sub>P/N-doped carbon composite nanosheet arrays as bifunctional electrocatalysts for hydrogen evolution and urea oxidation. *Chem. Eng. J.* **2021**, *408*, 127308. [[CrossRef](#)]
38. Alotaibi, N.; Hammud, H.H.; Al Otaibi, N.; Prakasam, T. Electrocatalytic properties of 3D hierarchical graphitic carbon-cobalt nanoparticles for urea oxidation. *ACS Omega* **2020**, *5*, 26038–26048. [[CrossRef](#)]
39. Xiao, C.; Li, S.; Zhang, X.; MacFarlane, D.R. MnO<sub>2</sub>/MnCo<sub>2</sub>O<sub>4</sub>/Ni heterostructure with quadruple hierarchy: A bifunctional electrode architecture for overall urea oxidation. *J. Mater. Chem. A* **2017**, *5*, 7825–7832. [[CrossRef](#)]
40. Elbohy, H.; Bahrami, B.; Mabrouk, S.; Reza, K.M.; Gurung, A.; Pathak, R.; Liang, M.; Qiao, Q.; Zhu, K. Tuning Hole transport layer using urea for high-performance perovskite solar cells. *Adv. Funct. Mater.* **2018**, *29*, 1806740. [[CrossRef](#)]
41. Li, P.; Zhuang, Z.; Du, C.; Xiang, D.; Zheng, F.; Zhang, Z.; Fang, Z.; Guo, J.; Zhu, S.; Chen, W. Insights into the Mo-doping effect on the electrocatalytic performance of hierarchical Co<sub>x</sub>Mo<sub>y</sub>S nanosheet arrays for hydrogen generation and urea oxidation. *ACS Appl. Mater. Interfaces* **2020**, *12*, 40194–40203. [[CrossRef](#)] [[PubMed](#)]
42. Chen, H.; Si, J.; Lyu, S.; Zhang, T.; Li, Z.; Lei, C.; Lei, L.; Yuan, C.; Yang, B.; Gao, L.; et al. Highly effective electrochemical exfoliation of ultrathin tantalum disulfide nanosheets for energy-efficient hydrogen evolution electrocatalysis. *ACS Appl. Mater. Interfaces* **2020**, *12*, 24675–24682. [[CrossRef](#)] [[PubMed](#)]
43. Chen, S.; Duan, J.; Vasileff, A.; Qiao, S.Z. Size fractionation of two-dimensional sub-nanometer thin manganese dioxide crystals towards superior urea electrocatalytic conversion. *Angew. Chem. Int. Ed.* **2016**, *55*, 3804–3808. [[CrossRef](#)] [[PubMed](#)]
44. Wang, Z.; Hu, Y.; Liu, W.; Xu, L.; Guan, M.; Zhao, Y.; Bao, J.; Li, H. Manganese-modulated cobalt-based layered double hydroxide grown on nickel foam with 1D-2D-3D heterostructure for highly efficient oxygen evolution reaction and urea oxidation reaction. *Chemistry* **2020**, *26*, 9382–9388. [[CrossRef](#)]
45. Liu, T.; Liu, D.; Qu, F.; Wang, D.; Zhang, L.; Ge, R.; Hao, S.; Ma, Y.; Du, G.; Asiri, A.M.; et al. Enhanced electrocatalysis for energy-efficient hydrogen production over CoP catalyst with nonelectroactive Zn as a promoter. *Adv. Energy Mater.* **2017**, *7*, 1700020. [[CrossRef](#)]
46. Sun, Y.; Duan, J.; Zhu, J.; Chen, S.; Antonietti, M. Metal-cluster-directed surface charge manipulation of two-dimensional nanomaterials for efficient urea electrocatalytic conversion. *ACS Appl. Nano Mater.* **2018**, *1*, 6649–6655. [[CrossRef](#)]
47. Vedharathinam, V.; Botte, G.G. Direct evidence of the mechanism for the electro-oxidation of urea on Ni(OH)<sub>2</sub> catalyst in alkaline medium. *Electrochim. Acta* **2013**, *108*, 660–665. [[CrossRef](#)]
48. Xu, W.; Zhang, H.; Li, G.; Wu, Z. Nickel-cobalt bimetallic anode catalysts for direct urea fuel cell. *Sci. Rep.* **2014**, *4*, 5863. [[CrossRef](#)]
49. Feng, Y.; Wang, X.; Huang, J.; Dong, P.; Ji, J.; Li, J.; Cao, L.; Feng, L.; Jin, P.; Wang, C. Decorating CoNi layered double hydroxides nanosheet arrays with fullerene quantum dot anchored on Ni foam for efficient electrocatalytic water splitting and urea electrolysis. *Chem. Eng. J.* **2020**, *390*, 124525. [[CrossRef](#)]
50. Xie, J.; Liu, W.; Zhang, X.; Guo, Y.; Gao, L.; Lei, F.; Tang, B.; Xie, Y. Constructing hierarchical wire-on-sheet nanoarrays in phase-regulated cerium-doped nickel hydroxide for promoted urea electro-oxidation. *ACS Mater. Lett.* **2019**, *1*, 103–110. [[CrossRef](#)]
51. Babar, P.; Lokhande, A.; Karade, V.; Pawar, B.; Gang, M.G.; Pawar, S.; Kim, J.H. Bifunctional 2D Electrocatalysts of transition metal hydroxide nanosheet arrays for water splitting and urea electrolysis. *ACS Sustain. Chem. Eng.* **2019**, *7*, 10035–10043. [[CrossRef](#)]
52. Sha, L.; Ye, K.; Yin, J.; Zhu, K.; Cheng, K.; Yan, J.; Wang, G.; Cao, D. In situ grown 3D hierarchical MnCo<sub>2</sub>O<sub>4.5</sub>@Ni(OH)<sub>2</sub> nanosheet arrays on Ni foam for efficient electrocatalytic urea oxidation. *Chem. Eng. J.* **2020**, *381*, 122603. [[CrossRef](#)]
53. Yue, Z.; Yao, S.; Li, Y.; Zhu, W.; Wang, R.; Wang, J.; Huang, L.; Zhao, D.; Wang, J. Surface engineering of hierarchical Ni(OH)<sub>2</sub> nanosheet@nanowire configuration toward superior urea electrolysis. *Electrochim. Acta* **2018**, *268*, 211–217. [[CrossRef](#)]
54. Zeng, M.; Wu, J.; Li, Z.; Wu, H.; Wang, J.; Wang, H.; He, L.; Yang, X. Interlayer effect in NiCo layered double hydroxide for promoted electrocatalytic urea oxidation. *ACS Sustain. Chem. Eng.* **2019**, *7*, 4777–4783. [[CrossRef](#)]
55. Wang, T.; Wu, H.; Feng, C.; Zhang, L.; Zhang, J. MoP@NiCo-LDH on nickel foam as bifunctional electrocatalyst for high efficiency water and urea–water electrolysis. *J. Mater. Chem. A* **2020**, *8*, 18106–18116. [[CrossRef](#)]
56. Meng, J.; Chernev, P.; Mohammadi, M.R.; Klingan, K.; Loos, S.; Pasquini, C.; Kubella, P.; Jiang, S.; Yang, X.; Cui, Z.; et al. Self-supported Ni(OH)<sub>2</sub>/MnO<sub>2</sub> on CFP as a flexible anode towards electrocatalytic urea conversion: The role of composition on activity, redox states and reaction dynamics. *Electrochim. Acta* **2019**, *318*, 32–41. [[CrossRef](#)]
57. Yan, X.; Hu, Q.-T.; Liu, J.; Zhang, W.-D.; Gu, Z.-G. Ultrafine-grained NiCo layered double hydroxide nanosheets with abundant active edge sites for highly enhanced electro-oxidation of urea. *Electrochim. Acta* **2021**, *368*, 137648. [[CrossRef](#)]
58. Sun, C.B.; Guo, M.W.; Siwal, S.S.; Zhang, Q.B. Efficient hydrogen production via urea electrolysis with cobalt doped nickel hydroxide-riched hybrid films: Cobalt doping effect and mechanism aspect. *J. Catal.* **2020**, *381*, 454–461. [[CrossRef](#)]
59. Xia, L.; Liao, Y.; Qing, Y.; Xu, H.; Gao, Z.; Li, W.; Wu, Y. In Situ growth of porous ultrathin ni(oh)<sub>2</sub> nanostructures on nickel foam: An efficient and durable catalysts for urea electrolysis. *ACS Appl. Energy Mater.* **2020**, *3*, 2996–3004. [[CrossRef](#)]
60. Xie, J.; Gao, L.; Cao, S.; Liu, W.; Lei, F.; Hao, P.; Xia, X.; Tang, B. Copper-incorporated hierarchical wire-on-sheet α-Ni(OH)<sub>2</sub> nanoarrays as robust trifunctional catalysts for synergistic hydrogen generation and urea oxidation. *J. Mater. Chem. A* **2019**, *7*, 13577–13584. [[CrossRef](#)]
61. Lan, R.; Tao, S.; Irvine, J.T.S. A direct urea fuel cell—Power from fertiliser and waste. *Energy Environ. Sci.* **2010**, *3*, 438. [[CrossRef](#)]
62. Yoon, J.; Lee, D.; Lee, Y.N.; Yoon, Y.S.; Kim, D.-J. Solid solution palladium-nickel bimetallic anode catalysts by co-sputtering for direct urea fuel cells (DUFC). *J. Power Sources* **2019**, *431*, 259–264. [[CrossRef](#)]

63. Ding, R.; Qi, L.; Jia, M.; Wang, H. Correction: Facile synthesis of mesoporous spinel NiCo<sub>2</sub>O<sub>4</sub> nanostructures as highly efficient electrocatalysts for urea electro-oxidation. *Nanoscale* **2015**, *7*, 9946. [[CrossRef](#)] [[PubMed](#)]
64. King, R.L.; Botte, G.G. Hydrogen production via urea electrolysis using a gel electrolyte. *J. Power Sources* **2011**, *196*, 2773–2778. [[CrossRef](#)]
65. Guo, F.; Cao, D.; Du, M.; Ye, K.; Wang, G.; Zhang, W.; Gao, Y.; Cheng, K. Enhancement of direct urea-hydrogen peroxide fuel cell performance by three-dimensional porous nickel-cobalt anode. *J. Power Sources* **2016**, *307*, 697–704. [[CrossRef](#)]
66. Yan, W.; Wang, D.; Botte, G.G. Nickel and cobalt bimetallic hydroxide catalysts for urea electro-oxidation. *Electrochim. Acta* **2012**, *61*, 25–30. [[CrossRef](#)]
67. Vidotti, M.; Silva, M.R.; Salvador, R.P.; de Torresi, S.I.C.; Dall'Antonia, L.H. Electrochemical oxidation of urea by nanostructured nickel/cobalt hydroxide electrodes. *Electrochim. Acta* **2008**, *53*, 4030–4034. [[CrossRef](#)]
68. Periyasamy, S.; Subramanian, P.; Levi, E.; Aurbach, D.; Gedanken, A.; Schechter, A. Exceptionally active and stable spinel nickel manganese oxide electrocatalysts for urea oxidation reaction. *ACS Appl. Mater. Interfaces* **2016**, *8*, 12176–12185. [[CrossRef](#)]
69. Barakat, N.A.M.; El-Newehy, M.H.; Yasin, A.S.; Ghouri, Z.K.; Al-Deyab, S.S. Ni&Mn nanoparticles-decorated carbon nanofibers as effective electrocatalyst for urea oxidation. *Appl. Catal. A Gen.* **2016**, *510*, 180–188.
70. Barakat, N.A.M.; Alajami, M.; Al Haj, Y.; Obaid, M.; Al-Meer, S. Enhanced onset potential NiMn-decorated activated carbon as effective and applicable anode in urea fuel cells. *Catal. Commun.* **2017**, *97*, 32–36. [[CrossRef](#)]
71. Vilana, J.; Gómez, E.; Vallés, E. Influence of the composition and crystalline phase of electrodeposited CoNi films in the preparation of CoNi oxidized surfaces as electrodes for urea electro-oxidation. *Appl. Surf. Sci.* **2016**, *360*, 816–825. [[CrossRef](#)]
72. Yan, W.; Wang, D.; Botte, G.G. Electrochemical decomposition of urea with Ni-based catalysts. *Appl. Catal. B Environ.* **2012**, *127*, 221–226. [[CrossRef](#)]
73. Kakati, N.; Maiti, J.; Lee, K.S.; Viswanathan, B.; Yoon, Y.S. Hollow sodium nickel fluoride nanocubes deposited MWCNT as an efficient electrocatalyst for urea oxidation. *Electrochim. Acta* **2017**, *240*, 175–185. [[CrossRef](#)]
74. Wang, L.; Du, T.; Cheng, J.; Xie, X.; Yang, B.; Li, M. Enhanced activity of urea electrooxidation on nickel catalysts supported on tungsten carbides/carbon nanotubes. *J. Power Sources* **2015**, *280*, 550–554. [[CrossRef](#)]
75. Vedharathinam, V.; Botte, G.G. Understanding the electro-catalytic oxidation mechanism of urea on nickel electrodes in alkaline medium. *Electrochim. Acta* **2012**, *81*, 292–300. [[CrossRef](#)]
76. Xu, W.; Du, D.; Lan, R.; Humphreys, J.; Wu, Z.; Tao, S. Highly active Ni-Fe double hydroxides as anode catalysts for electrooxidation of urea. *New J. Chem.* **2017**, *41*, 4190–4196. [[CrossRef](#)]
77. Abdelkareem, M.A.; Al Haj, Y.; Alajami, M.; Alawadhi, H.; Barakat, N.A.M. Ni-Cd carbon nanofibers as an effective catalyst for urea fuel cell. *J. Environ. Chem. Eng.* **2018**, *6*, 332–337. [[CrossRef](#)]
78. Kim, B.; Das, G.; Park, B.J.; Lee, D.H.; Yoon, H.H. A free-standing NiCr-CNT@C anode mat by electrospinning for a high-performance urea/H<sub>2</sub>O<sub>2</sub> fuel cell. *Electrochim. Acta* **2020**, *354*, 136657. [[CrossRef](#)]
79. Singh, R.K.; Schechter, A. Electroactivity of NiCr catalysts for urea oxidation in alkaline electrolyte. *ChemCatChem* **2017**, *9*, 3374–3379. [[CrossRef](#)]
80. Mohamed, I.M.A.; Yasin, A.S.; Barakat, N.A.M.; Song, S.A.; Lee, H.E.; Kim, S.S. Electrochemical behavior of a nanocomposite of Ni/Pd supported by carbonized PVA nanofibers towards formic acid, ethanol and urea oxidation: A physicochemical and electro-analysis study. *Appl. Surf. Sci.* **2018**, *435*, 122–129. [[CrossRef](#)]
81. Sun, H.; Zhang, W.; Li, J.-G.; Li, Z.; Ao, X.; Xue, K.-H.; Ostrikov, K.K.; Tang, J.; Wang, C. Rh-engineered ultrathin NiFe-LDH nanosheets enable highly-efficient overall water splitting and urea electrolysis. *Appl. Catal. B Environ.* **2021**, *284*, 119740. [[CrossRef](#)]
82. Xu, Y.; Chai, X.; Ren, T.; Yu, S.; Yu, H.; Wang, Z.; Li, X.; Wang, L.; Wang, H. Ir-Doped Ni-based metal-organic framework ultrathin nanosheets on Ni foam for enhanced urea electro-oxidation. *Chem. Commun.* **2020**, *56*, 2151–2154. [[CrossRef](#)] [[PubMed](#)]
83. Khalafallah, D.; Xiaoyu, L.; Zhi, M.; Hong, Z. 3D Hierarchical NiCo layered double hydroxide nanosheet arrays decorated with noble metal nanoparticles for enhanced urea electrocatalysis. *ChemElectroChem* **2019**, *7*, 163–174. [[CrossRef](#)]
84. Wang, D.; Yan, W.; Vijapur, S.H.; Botte, G.G. Enhanced electrocatalytic oxidation of urea based on nickel hydroxide nanoribbons. *J. Power Sources* **2012**, *217*, 498–502. [[CrossRef](#)]
85. Ye, K.; Zhang, D.; Guo, F.; Cheng, K.; Wang, G.; Cao, D. Highly porous nickel@carbon sponge as a novel type of three-dimensional anode with low cost for high catalytic performance of urea electro-oxidation in alkaline medium. *J. Power Sources* **2015**, *283*, 408–415. [[CrossRef](#)]
86. Guo, F.; Ye, K.; Cheng, K.; Wang, G.; Cao, D. Preparation of nickel nanowire arrays electrode for urea electro-oxidation in alkaline medium. *J. Power Sources* **2015**, *278*, 562–568. [[CrossRef](#)]
87. Yan, W.; Wang, D.; Diaz, L.A.; Botte, G.G. Nickel nanowires as effective catalysts for urea electro-oxidation. *Electrochim. Acta* **2014**, *134*, 266–271. [[CrossRef](#)]
88. Zhang, J.-Y.; He, T.; Wang, M.; Qi, R.; Yan, Y.; Dong, Z.; Liu, H.; Wang, H.; Xia, B.Y. Energy-saving hydrogen production coupling urea oxidation over a bifunctional nickel-molybdenum nanotube array. *Nano Energy* **2019**, *60*, 894–902. [[CrossRef](#)]
89. Cao, J.; Li, H.; Zhu, R.; Ma, L.; Zhou, K.; Wei, Q.; Luo, F. Improved hydrogen generation via a urea-assisted method over 3D hierarchical NiMo-based composite microrod arrays. *J. Alloy. Compd.* **2020**, *844*, 155382. [[CrossRef](#)]
90. Mohamed, I.M.A.; Liu, C. Chemical design of novel electrospun CoNi/Cr nanoparticles encapsulated in C-nanofibers as highly efficient material for urea oxidation in alkaline media. *Appl. Surf. Sci.* **2019**, *475*, 532–541. [[CrossRef](#)]

91. Gao, X.; Wang, Y.; Li, W.; Li, F.; Arandiyani, H.; Sun, H.; Chen, Y. Free-standing Ni-Co alloy nanowire arrays: Efficient and robust catalysts toward urea electro-oxidation. *Electrochim. Acta* **2018**, *283*, 1277–1283. [[CrossRef](#)]
92. Wu, M.-S.; Jao, C.-Y.; Chuang, F.-Y.; Chen, F.-Y. Carbon-encapsulated nickel-iron nanoparticles supported on nickel foam as a catalyst electrode for urea electrolysis. *Electrochim. Acta* **2017**, *227*, 210–216. [[CrossRef](#)]
93. Nangan, S.; Ding, Y.; Alhakemy, A.Z.; Liu, Y.; Wen, Z. Hybrid alkali-acid urea-nitrate fuel cell for degrading nitrogen-rich wastewater. *Appl. Catal. B Environ.* **2021**, *286*, 119892. [[CrossRef](#)]
94. Singh, R.K.; Subramanian, P.; Schechter, A. enhanced urea activity of oxidation on nickel-deposited tin dendrites. *ChemElectroChem* **2017**, *4*, 1037–1043. [[CrossRef](#)]
95. Wang, S.; Xu, P.; Tian, J.; Liu, Z.; Feng, L. Phase structure tuning of graphene supported Ni-NiO Nanoparticles for enhanced urea oxidation performance. *Electrochim. Acta* **2021**, *370*, 137755. [[CrossRef](#)]
96. Liu, M.; Jiao, Y.; Zhan, S.; Wang, H. Ni<sub>3</sub>S<sub>2</sub> nanowires supported on Ni foam as efficient bifunctional electrocatalyst for urea-assisted electrolytic hydrogen production. *Catal. Today* **2020**, *355*, 596–601. [[CrossRef](#)]
97. Xu, B.; Yang, X.; Liu, X.; Song, W.; Sun, Y.; Liu, Q.; Yang, H.; Li, C. Lattice distortion in hybrid NiTe<sub>2</sub>/Ni(OH)<sub>2</sub> nanosheets as efficient synergistic electrocatalyst for water and urea oxidation. *J. Power Sources* **2020**, *449*, 227585. [[CrossRef](#)]
98. Li, M.; Ao, X.; Li, J.-G.; Sun, H.; Zheng, L.; Wang, C. NiCo-BDC nanosheets coated with amorphous Ni-S thin film for high-efficiency oxygen evolution reaction and urea oxidation reaction. *FlatChem* **2021**, *25*, 100222. [[CrossRef](#)]
99. Song, W.; Xu, M.; Teng, X.; Niu, Y.; Gong, S.; Liu, X.; He, X.; Chen, Z. Construction of self-supporting, hierarchically structured caterpillar-like NiCo<sub>2</sub>S<sub>4</sub> arrays as an efficient trifunctional electrocatalyst for water and urea electrolysis. *Nanoscale* **2021**, *13*, 1680–1688. [[CrossRef](#)]
100. Lu, S.; Gu, Z.; Hummel, M.; Zhou, Y.; Wang, K.; Xu, B.B.; Wang, Y.; Li, Y.; Qi, X.; Liu, X. Nickel Oxide Immobilized on the Carbonized Eggshell Membrane for Electrochemical Detection of Urea. *J. Electrochem. Soc.* **2020**, *167*, 106509. [[CrossRef](#)]
101. Wang, Z.; Guo, P.; Liu, M.; Guo, C.; Liu, H.; Wei, S.; Zhang, J.; Lu, X. Rational design of metallic NiTe<sub>x</sub> (x = 1 or 2) as bifunctional electrocatalysts for efficient urea conversion. *ACS Appl. Energy Mater.* **2019**, *2*, 3363–3372. [[CrossRef](#)]
102. Hu, S.; Wang, S.; Feng, C.; Wu, H.; Zhang, J.; Mei, H. Novel MOF-derived nickel nitride as high-performance bifunctional electrocatalysts for hydrogen evolution and urea oxidation. *ACS Sustain. Chem. Eng.* **2020**, *8*, 7414–7422. [[CrossRef](#)]
103. Liu, Q.; Xie, L.; Qu, F.; Liu, Z.; Du, G.; Asiri, A.M.; Sun, X. A porous Ni<sub>3</sub>N nanosheet array as a high-performance non-noble-metal catalyst for urea-assisted electrochemical hydrogen production. *Inorg. Chem. Front.* **2017**, *4*, 1120–1124. [[CrossRef](#)]
104. Khalafallah, D.; Zhi, M.; Hong, Z. Shape-dependent electrocatalytic activity of carbon reinforced Ni<sub>2</sub>P hybrids toward urea electrocatalysis. *Energy Technol.* **2019**, *7*, 1900548. [[CrossRef](#)]
105. Wang, G.; Ye, K.; Shao, J.; Zhang, Y.; Zhu, K.; Cheng, K.; Yan, J.; Wang, G.; Cao, D. Porous Ni<sub>2</sub>P nanoflower supported on nickel foam as an efficient three-dimensional electrode for urea electro-oxidation in alkaline medium. *Int. J. Hydrog. Energy* **2018**, *43*, 9316–9325. [[CrossRef](#)]
106. Liu, H.; Liu, Z.; Wang, F.; Feng, L. Efficient catalysis of N doped NiS/NiS<sub>2</sub> heterogeneous structure. *Chem. Eng. J.* **2020**, *397*, 125507. [[CrossRef](#)]
107. He, M.; Feng, C.; Liao, T.; Hu, S.; Wu, H.; Sun, Z. Low-cost Ni<sub>2</sub>P/Ni<sub>0.96</sub>S heterostructured bifunctional electrocatalyst toward highly efficient overall urea-water electrolysis. *ACS Appl. Mater. Interfaces* **2020**, *12*, 2225–2233. [[CrossRef](#)]
108. Zhang, Y.; Qiu, Y.; Wang, Y.; Li, B.; Zhang, Y.; Ma, Z.; Liu, S. Coaxial Ni-S@N-doped carbon nanofibers derived hierarchical electrodes for efficient H<sub>2</sub> production via urea electrolysis. *ACS Appl. Mater. Interfaces* **2021**, *13*, 3937–3948. [[CrossRef](#)]
109. Wang, L.; Cao, J.; Lei, C.; Dai, Q.; Yang, B.; Li, Z.; Zhang, X.; Yuan, C.; Lei, L.; Hou, Y. Strongly coupled 3D N-doped MoO<sub>2</sub>/Ni<sub>3</sub>S<sub>2</sub> hybrid for high current density hydrogen evolution electrocatalysis and biomass upgrading. *ACS Appl. Mater. Interfaces* **2019**, *11*, 27743–27750. [[CrossRef](#)]
110. Wu, F.; Ou, G.; Yang, J.; Li, H.; Gao, Y.; Chen, F.; Wang, Y.; Shi, Y. Bifunctional nickel oxide-based nanosheets for highly efficient overall urea splitting. *Chem. Commun.* **2019**, *55*, 6555–6558. [[CrossRef](#)]
111. Sha, L.; Yin, J.; Ye, K.; Wang, G.; Zhu, K.; Cheng, K.; Yan, J.; Wang, G.; Cao, D. The construction of self-supported thorny leaf-like nickel-cobalt bimetal phosphides as efficient bifunctional electrocatalysts for urea electrolysis. *J. Mater. Chem. A* **2019**, *7*, 9078–9085. [[CrossRef](#)]
112. Han, W.K.; Li, X.P.; Lu, L.N.; Ouyang, T.; Xiao, K.; Liu, Z.Q. Partial S substitution activates NiMoO<sub>4</sub> for efficient and stable electrocatalytic urea oxidation. *Chem. Commun.* **2020**, *56*, 11038–11041. [[CrossRef](#)] [[PubMed](#)]
113. Rezaee, S.; Shahrokhian, S. 3D ternary Ni<sub>x</sub>Co<sub>2-x</sub>P/C nanoflower/nanourchin arrays grown on HCNs: A highly efficient bi-functional electrocatalyst for boosting hydrogen production via the urea electro-oxidation reaction. *Nanoscale* **2020**, *12*, 16123–16135. [[CrossRef](#)] [[PubMed](#)]
114. Li, J.; Yao, C.; Kong, X.; Li, Z.; Jiang, M.; Zhang, F.; Lei, X. Boosting hydrogen production by electrooxidation of urea over 3d hierarchical Ni<sub>4</sub>N/Cu<sub>3</sub>N nanotube arrays. *ACS Sustain. Chem. Eng.* **2019**, *7*, 13278–13285. [[CrossRef](#)]
115. Zhu, W.; Ren, M.; Hu, N.; Zhang, W.; Luo, Z.; Wang, R.; Wang, J.; Huang, L.; Suo, Y.; Wang, J. Traditional NiCo<sub>2</sub>S<sub>4</sub> phase with porous nanosheets array topology on carbon cloth: A flexible, versatile and fabulous electrocatalyst for overall water and urea electrolysis. *ACS Sustain. Chem. Eng.* **2018**, *6*, 5011–5020. [[CrossRef](#)]
116. Wang, L.; Liu, Z.; Zhu, S.; Shao, M.; Yang, B.; Chen, J.G. Tungsten carbide and cobalt modified nickel nanoparticles supported on multiwall carbon nanotubes as highly efficient electrocatalysts for urea oxidation in alkaline electrolyte. *ACS Appl. Mater. Interfaces* **2018**, *10*, 41338–41343. [[CrossRef](#)]

117. Wang, L.; Ren, L.; Wang, X.; Feng, X.; Zhou, J.; Wang, B. Multivariate MOF-templated pomegranate-Like Ni/C as efficient bifunctional electrocatalyst for hydrogen evolution and urea oxidation. *ACS Appl. Mater. Interfaces* **2018**, *10*, 4750–4756. [[CrossRef](#)]
118. Zhang, Q.; Kazim, F.M.D.; Ma, S.; Qu, K.; Li, M.; Wang, Y.; Hu, H.; Cai, W.; Yang, Z. Nitrogen dopants in nickel nanoparticles embedded carbon nanotubes promote overall urea oxidation. *Appl. Catal. B Environ.* **2021**, *280*, 119436. [[CrossRef](#)]
119. Munde, A.V.; Mulik, B.B.; Chavan, P.P.; Sathe, B.R. Enhanced electrocatalytic activity towards urea oxidation on Ni nanoparticle decorated graphene oxide nanocomposite. *Electrochim. Acta* **2020**, *349*, 136386. [[CrossRef](#)]
120. Zhang, L.; Wang, L.; Lin, H.; Liu, Y.; Ye, J.; Wen, Y.; Chen, A.; Wang, L.; Ni, F.; Zhou, Z.; et al. A lattice-oxygen-involved reaction pathway to boost urea oxidation. *Angew. Chem. Int. Ed. Engl.* **2019**, *58*, 16820–16825. [[CrossRef](#)]
121. Wang, C.; Lu, H.; Mao, Z.; Yan, C.; Shen, G.; Wang, X. Bimetal schottky heterojunction boosting energy-saving hydrogen production from alkaline water via urea electrocatalysis. *Adv. Funct. Mater.* **2020**, *30*, 2000556. [[CrossRef](#)]
122. He, Q.; Wan, Y.; Jiang, H.; Pan, Z.; Wu, C.; Wang, M.; Wu, X.; Ye, B.; Ajayan, P.M.; Song, L. Nickel vacancies boost reconstruction in nickel hydroxide electrocatalyst. *ACS Energy Lett.* **2018**, *3*, 1373–1380. [[CrossRef](#)]
123. Tong, Y.; Chen, P.; Zhang, M.; Zhou, T.; Zhang, L.; Chu, W.; Wu, C.; Xie, Y. oxygen vacancies confined in nickel molybdenum oxide porous nanosheets for promoted electrocatalytic urea oxidation. *ACS Catal.* **2017**, *8*, 1–7. [[CrossRef](#)]